TABLE 1
Sequences of Primers and Annealing Temperatures Used for Real-Time RT-PCR Analyses

Target	Primer	Sequence	Annealing temperature (°C)
T-bet	FP	5′-CAA GTG GGT GCA GTG TGG AAA G-3′	68
	RP	5′-TGG AGA GAC TGC AGG ACG ATC-3′	
GATA-3	FP	5′-GGA GGA CTT CCC CAA GAG CA-3′	62
	RP	5′-CAT GCT GGA AGG GTG GTG A-3′	
IFN-γ	FP	5′-GGC CAT CAG CAA CAT AAG C-3′	68
	RP	5′-TGG ACC ACT CGG ATG AGC TCA-3′	
IL-10	FP	5′-TGA AGA CCC TCA GGA TGC GG-3′	66
	RP	5′-AGA GCT CTG TCT AGG TCC TGG-3′	
TNF-α	FP	5′-TGT CTC AGC CTC TTC TCA TTC C-3′	66
	RP	5′-TGA GGG TCT GGG CCA TAG AAC-3′	
MIP-2	FP	5′-AAG TTT GCC TTG ACC CTG AAG-3′	64
	RP	5′-ATC AGG TAC GAT CCA GGC TTC-3′	
β-Actin	FP	5′-ACG GCC AGG TCA TCA CTA TTG G-3′	68
	RP	5′-CTA GGA GCC AGA GCA GTA ATC TC-3′	

Note. FP, forward primer; RP, reverse primer.

chemokines, and thus has an important role in neutrophil infiltration and activation. Th17 cytokines secreted by T cells are suppressed by Th-2-dominant cytokines (Gu *et al.*, 2008) suggesting some involvement of IL-17.

Liver inflammation mediated by neutrophils has been demonstrated in some experimental animal models showing ethanol-, acetaminophen-, and α-naphthyl-isothiocyanate–induced liver inflammation and ischemia-reperfusion liver injury (Ramaiah and Jaeschke, 2007). Although, the role of neutrophils in the pathogenesis of halothane-induced liver injury was demonstrated previously (You *et al.*, 2006), Th cell involvement, which has been implicated as critical in some autoimmune diseases (Zhu and Paul, 2008), remains unknown. In this study, we investigated whether Th cells play an important role in halothane-induced liver injury. First, the expressions of transcription factors and cytokines specific for Th1 and Th2, respectively, were compared between susceptible and tolerant mice strains. Second, to investigate IL-17 involvement, the plasma IL-17 level was measured, and neutralization and administration of recombinant IL-17 were performed.

MATERIALS AND METHODS

Chemicals. Halothane was purchased from Sigma (St Louis, MO). Transaminase CII-test Wako was from Wako Pure Chemical Industries (Osaka, Japan). RNAiso was from Nippon Gene (Tokyo, Japan). ReverTra Ace was from Toyobo (Tokyo, Japan). Random hexamer and SYBR Premix Ex Taq were from Takara (Osaka, Japan). All primers were commercially synthesized at Hokkaido System Sciences (Sapporo, Japan). Prostaglandin E_1 (PGE_1) was purchased from Nippon Chemiphar (Tokyo, Japan). Monoclonal anti-mouse IL-17 antibody, rat IgG2a isotype and recombinant mouse IL-17 were from R&D Systems (Abingdon, UK). A Ready-SET-GO! Mouse Interleukin-17A (IL-17A) enzyme-linked immunosorbent assay (ELISA) kit was from eBioscience (San Diego, CA). Other chemicals were of analytical or the highest grade commercially available.

Halothane administration. Female BALB/cCrSlc mice and C57BL/6JJmsSlc (6–7 weeks old, 15–21 g) were obtained from SLC Japan (Hamamatsu, Japan). Animals were housed in a controlled environment (temperature 25 ± 1°C, humidity 50 ± 10%, and 12-h light/12-h dark cycle) in the institutional animal facility with access to food and water *ad libitum*. Animals were acclimatized before use for the experiments. Mice were administered ip halothane (600 μmol per mouse, dissolved in 2 ml of olive oil) in a nonfasting condition. At 3, 6, 12, and 24 h after halothane administration, the animals were sacrificed and the blood and the liver were collected. For measurement of the plasma IL-17 level, mice were sacrificed at 1, 3, 6, 9, 12, and 24 h after the halothane administration. A portion of each excised liver was fixed in 10% formalin neutral buffer solution and used for immunohistochemical staining. The degree of liver injury was assessed by hematoxylin-eosin (H&E) staining and plasma aspartate aminotransferase (AST) and alanine aminotransferase (ALT) levels were measured by Transaminase CII-test Wako according to the manufacturer's instructions. The neutrophil infiltration was assessed by immunostaining for the myeloperoxidase (MPO). Animal maintenance and treatment were conducted in accordance with the National Institutes of Health Guide for Animal Welfare of Japan, as approved by the Institutional Animal Care and Use Committee of Kanazawa University, Japan.

Real-time RT-PCR. RNA from the mouse liver was isolated using RNAiso according to the manufacturer's instructions. T-bet, GATA-3, IFN-γ, IL-10, tumor necrosis factor α (TNF-α), macrophage inflammatory ptrotein-2 (MIP-2), and β-actin were quantified by real-time RT-PCR. The primer sequences used in this study are shown in Table 1. For the RT-process, total RNA (10 μg) and 150 ng random hexamer were mixed and incubated at 70°C for 10 min. RNA solution was added to a reaction mixture containing 100 units of ReverTra Ace (Reverse transcriptase, TOYOBO, Tokyo, Japan), reaction buffer and 0.5mM deoxy-nucleotide triphosphates in a final volume of 40 μl. The reaction mixture was incubated at 30°C for 10 min, 42°C for 1 h, and heated at 98°C for 10 min to inactivate the enzyme. The real-time RT-PCR was performed using the Mx3000P (Stratagene, La Jolla, CA). The PCR mixture contained 1 or 2 μl of template cDNA, SYBR Premix Ex Taq solution, and 8 pmol of forward and reverse primers. Amplified products were monitored directly by measuring the increase of the dye intensity of the SYBR Green I (Molecular Probes, Eugene, OR) that binds to the double-strand DNA amplified by PCR.

Administration of anti-mouse IL-17 antibody or recombinant mouse IL-17. Nine hours after halothane administration, mice were administered anti-mouse IL-17 antibody intraperitoneally (100 μg of anti-mouse IL-17 antibody in 0.5 ml of sterile phosphate buffered saline [PBS]) in nonfasting condition. As a control, rat IgG2a was administered (100 μg of rat IgG2a in 0.5 ml of sterile PBS). One hour before halothane administration, recombinant

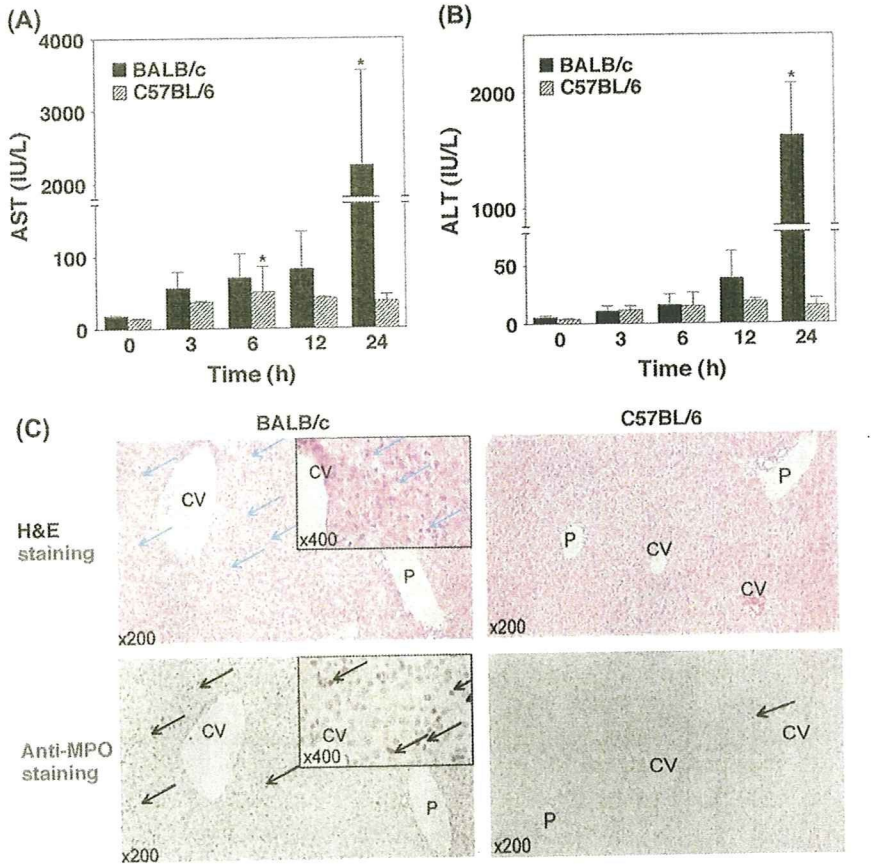

FIG. 1. Change of plasma AST and ALT levels and histological presentation of liver injury in halothane-administrated mice. Mice were administrated halothane (600 μmol per mouse, ip), and plasma for the AST (A) and ALT (B) assay were collected 3, 6, 12, and 24 h after administration. The data are means ± SD of 5–14 mice. Significantly different from control group (*$p < 0.05$). Liver specimens were sampled 24 h after halothane administration (C). Then, liver tissue sections were stained with H&E or immunostained with anti-MPO antibody. Arrows indicated necrotic cells and MPO-positive cells. CV, central vein; P, portal vein.

mouse IL-17 was intraperitoneally administered (1 μg of recombinant IL-17 in 0.2 ml of sterile PBS containing 0.5% BSA) in nonfasting condition. As a control, vehicle was administered.

Treatment of PGE_1. Six, 9, or 12 h after halothane administration, mice were treated with PGE_1 intraperitoneally (50 μg/20 g bw, dissolved in 500 μl of sterile saline) in nonfasting condition. As a control, vehicle was administered.

Measurement of plasma IL-17 level. The plasma IL-17 level was measured by ELISA using a Ready-SET-GO! Mouse IL-17A kit from eBioscience (San Diego, CA) according to the manufacturer's instructions.

Statistical analysis. Data are presented as mean ± SD. Statistical analyses between multiple groups were performed using one-way ANOVA with a *post hoc* test of significance between individual groups. Comparisons between two groups were carried out using two-tailed Student's *t*-test. $p < 0.05$ was considered statistically significant.

RESULTS

Increase of Plasma AST and ALT Levels in Halothane-Administrated BALB/c Mice

Female BALB/c and C57BL/6 mice were administered halothane at a dose of 600 μmol per mouse. Halothane administration resulted in a slight increase of the plasma AST and ALT levels in C57BL/6 mice, whereas a marked increase of the AST and ALT levels was observed 24 h after the administration in BALB/c mice (Figs. 1A and 1B).

Infiltration of Neutrophils in BALB/c Mouse Liver after Halothane Administration

Liver histology demonstrated that C57BL/6 mice had normal liver architecture, whereas focal necrosis in the centrilobular areas was observed in BALB/c mouse liver (Fig. 1C). In addition, immunohistochemical analysis with anti-MPO antibody demonstrated that a number of MPO-positive cells had infiltrated in BALB/c mouse liver at 24 h after halothane administration.

Expression of Transcription Factors and Cytokines Genes in Halothane-Administered Mouse Liver

To investigate the involvement of Th cells in the induction of halothane hepatotoxicity, hepatic mRNA of T-bet, GATA-3, IFN-γ, and IL-10 were measured by real-time RT-PCR. It was

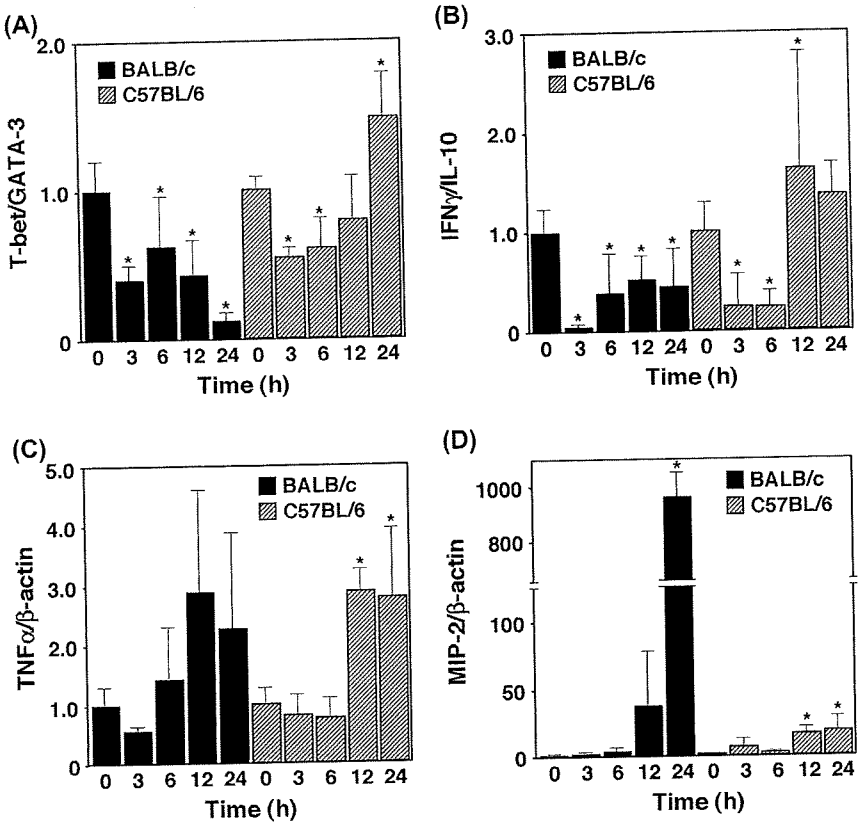

FIG. 2. Changes of hepatic mRNA expression in halothane-administrated mice. Mice were administrated halothane (600 μmol per mouse, ip). After 3, 6, 12, and 24 h, relative expression of hepatic mRNA was measured for T-bet/GATA-3 (A), IFN-γ/IL-10 (B), TNF-α/β-actin (C), and MIP-2/β-actin (D) by real-time RT-PCR. The data are means ± SD of three mice. Significantly different from control group (*$p < 0.05$).

suggested that the mRNA expression ratio of T-bet/GATA-3 and IFN-γ/IL-10 rather than the expression of either transcription factor alone reflected more closely in the Th1/Th2 cytokine balance (Chakir *et al.*, 2003). The T-bet/GATA-3 mRNA expression ratio was decreased at all time points after the administration of halothane in BALB/c mice, whereas the ratio was low at around 3–6 h and relatively high at 12–24 h in C57BL/6 mice (Fig. 2A). The IFN-γ/IL-10 mRNA expression ratio became similar to the T-bet/GATA-3 mRNA expression ratio (Fig. 2B). The T-bet/GATA-3 and IFN-γ/IL-10 mRNA expression ratio was lower in BALB/c mice compared with C57BL/6 mice. From these results, a typical Th1- or Th2-dominant response could not be distinguished. However, the mRNA expression of GATA-3 and IL-10 was relatively increased in BALB/c mice compared with C57BL/6 mice.

Measurement of Proinflammatory Cytokine and CXC Chemokine

To investigate whether the changes in liver injury and neutrophil infiltration observed in halothane-administered BALB/c mice resulted from increases of proinflammatory cytokine and CXC chemokine, we measured hepatic TNF-α and MIP-2 mRNA expression. TNF-α was slightly increased in both strains (Fig. 2C). At 12 and 24 h after halothane administration in BALB/c mice, a high SD value was observed. Thus, from these results, no conclusion about the involvement of TNF-α could be drawn (Fig. 2C). MIP-2 was markedly increased in BALB/c mice 24 h after halothane administration (Fig. 2D). These results suggested that MIP-2 may be involved in the neutrophil infiltration.

Time-Dependent Changes of Plasma Il-17 Level in Halothane Administered Mice, and Effects of Anti-IL-17 Antibody Administration

IL-17 is a cytokine produced by the newly defined Th cell subset Th17 which has inflammatory effects. To investigate whether IL-17 was involved in the infiltration of neutrophils in halothane-induced liver injury, we conducted a set of neutralization studies. Before the neutralization study, time-dependent changes of the plasma IL-17 level were measured. Mice were administered ip halothane (600 μmol per mouse) in nonfasting condition. The IL-17 level was significantly increased only 24 h after the halothane administration (Fig. 3A). ALT and AST were significantly increased in BALB/c mice as

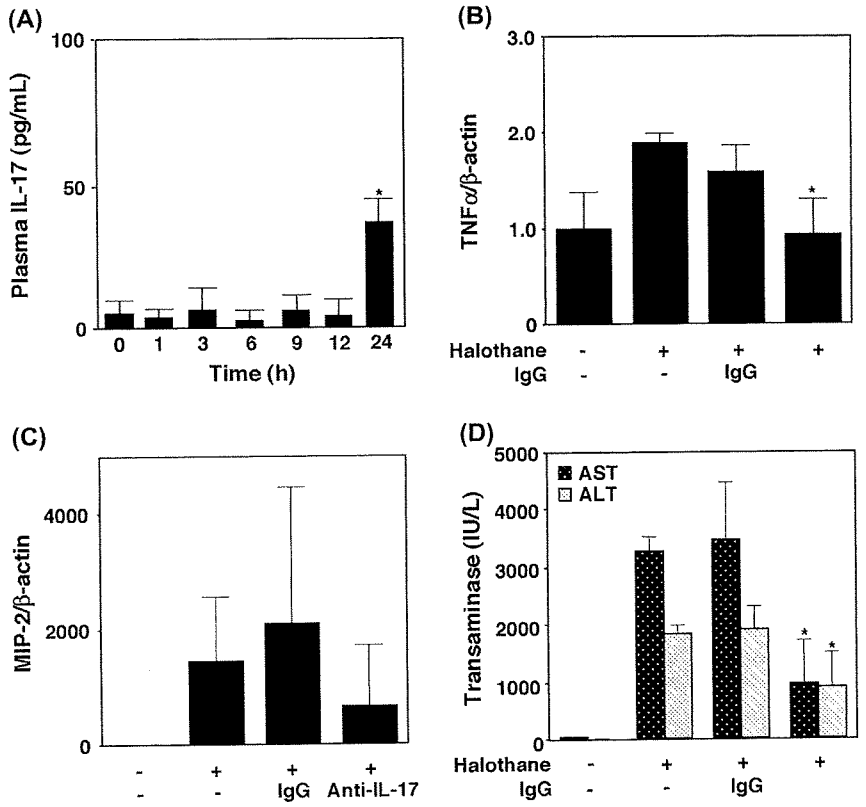

FIG. 3. Effect of anti-mouse IL-17 antibody administration on hepatic mRNA expression and plasma AST and ALT levels in halothane-administrated BALB/c mice. Mice were administrated halothane (600 μmol per mouse, ip). Plasma IL-17 level was measured 1, 3, 6, 9, 12, and 24 h after the halothane administration (A). Some mice were administrated with anti-mouse IL-17 antibody (100 μg per mouse, ip) or with rat IgG2a 9 h after the halothane administration. Twenty-four hours after halothane administration, relative expression of hepatic mRNA was measured for TNF-α/β-actin (B), and MIP-2/β-actin (C) by real-time RT-PCR. Plasma for the AST and ALT assay were collected 24 h after the halothane administration (D). The data are means ± SD of three to five mice. Significantly different from halothane- plus IgG2a-administrated group (*$p < 0.05$).

demonstrated in Figures 1A and 1B. In the neutralization study, the ip administration of a specific anti-mouse IL-17 antibody 9 h after halothane administration reduced hepatic TNF-α mRNA increases and plasma AST and ALT levels at 24 h after halothane administration (Figs. 3B and 3D). The expression of MIP-2 mRNA showed a tendency to decrease by the anti-IL-17 antibody administration (Fig. 3C). These inhibitory effects were not observed by the administration of rat IgG2a. As a preliminary study, we investigated to find the appropriate time for the administration of anti-IL-17 antibody at 3, 6, and 9 h after the halothane administration, as well as one hour before the halothane administration. As a result, the 9-h group showed the lowest expression levels of hepatic TNF-α, MIP-2 mRNA, AST, and ALT (data not shown). These results indicated that the halothane-induced liver injury was significantly suppressed by the administration of anti-IL-17 antibody.

Exacerbation of Hepatotoxic Effect by Recombinant IL-17 Administration

To further investigate whether IL-17 was involved in the halothane-induced liver injury, we performed a recombinant mouse IL-17 administration study. The ip administration of recombinant IL-17 at 1 h before the halothane administration caused remarkable increases of plasma aminotransferases at 12 and 24 h after halothane administration (Fig. 4A). To clarify the exacerbation of the hepatotoxic effect by the administration of recombinant IL-17, the dose of halothane was decreased to one half (300 μmol per mouse, ip) in this experiment. This dose of halothane (300 μmol per mouse) caused almost no increase of the plasma ALT and AST levels (data not shown). In the recombinant IL-17 and halothane-administered mice, the plasma IL-17 level remained relatively high (Fig. 4B). In the recombinant IL-17 and no-halothane–administered mice, the plasma IL-17 level was decreased to the same level as the nontreated mice indicating that the recombinant IL-17 had decreased completely at 24 h after the halothane adiministration.

Effect of Prostaglandin E_1 Treatment on Plasma IL-17 Level

Prostaglandins E series (PGEs) are known to protect against drug-induced and immune-mediated liver injury by down-regulating the production of inflammatory cytokines. It was reported that the Th2-like response of liver T cells might

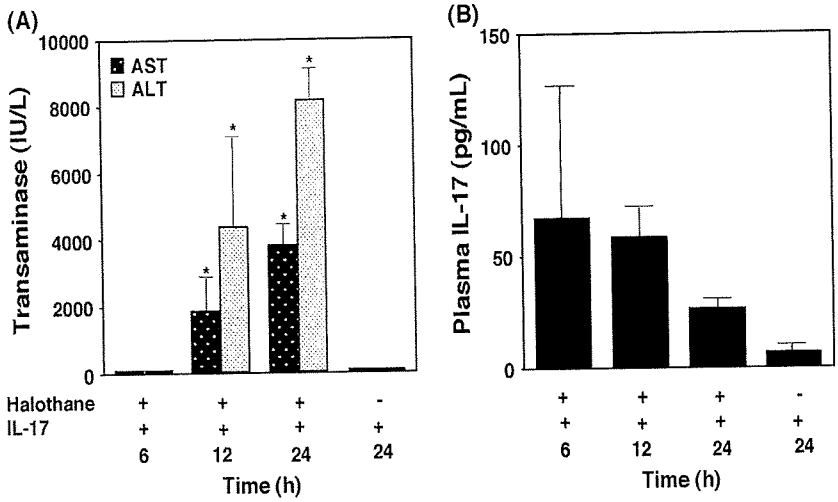

FIG. 4. Effect of recombinant mouse IL-17 administration on plasma AST, ALT, and IL-17 levels in halothane-administrated BALB/c mice. Mice were administrated halothane (300 μmol per mouse, ip). One hour before the halothane administration, recombinant mouse IL-17 (1 μg per mouse, ip) was administered. After 6, 12, and 24 h, plasma AST, ALT, and IL-17 levels were measured. The data are means ± SD of three to five mice. Significantly different from 6-h group (*$p < 0.05$).

involved in the mechanism whereby PGE_1 protects against liver injury (Mokuno *et al.*, 1999). PGE_1 inhibited the functions of neutrophils (Talpain *et al.*, 1995). However, the effect of PGE_1 on the plasma IL-17 level was not elucidated. To investigate the effect of PGE_1 on the plasma IL-17 level, PGE_1 conjugated by α-cyclodextrin was intraperitoneally administered to BALB/c mice and the plasma IL-17 level was measured by using ELISA. The plasma IL-17 level was increased in BALB/c mice 24 h after halothane administration and significantly inhibited by PGE_1 administration, whereas no change was observed in C57BL/6 mice (Fig. 5). The increase of the plasma IL-17 level in BALB/c mice suggested that this cytokine may account for strain differences in the susceptibility to halothane-induced liver injury.

Inhibition of Hepatic TNF-α and MIP-2 mRNA Expression in PGE_1-Treated Mice

We next investigated whether the hepatic expression of proinflammatory cytokines and CXC chemokines are changed in PGE_1-treated mice. The hepatic MIP-2 mRNA expression 24 h after halothane administration was significantly inhibited by treatment with PGE_1, whereas the TNF-α increase was not affected by PGE_1 (Figs. 6A and 6B). These results suggested that PGE_1 could inhibit the increase of MIP-2 expression via IL-17 signaling.

Protective Effect of PGE_1 Treatment Against Halothane-Induced Liver Injury

To investigate the protective effect of PGE_1 on the halothane-induced liver injury, we treated BALB/c mice with PGE_1, and measured the plasma AST and ALT levels 24 h after halothane administration. PGE_1 treatment significantly inhibited the increase of the plasma AST and ALT levels by halothane in BALB/c mice 9 h after halothane administration (Fig. 6C). Therefore, PGE_1 demonstrated a protective effect against halothane-induced liver injury in BALB/c mice.

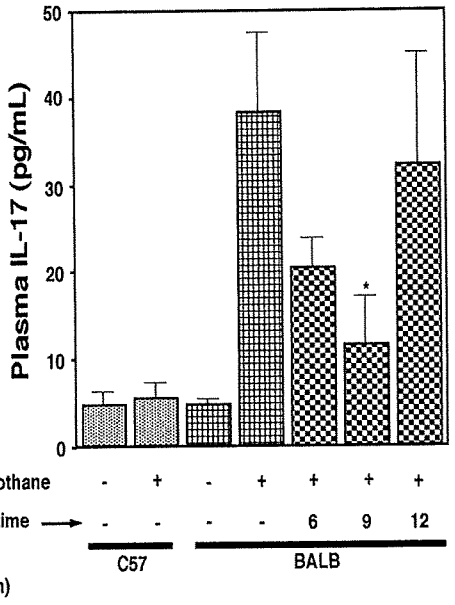

FIG. 5. Effect of PGE_1 treatment on plasma IL-17 level in halothane-administrated mice. Mice were administrated halothane (600 μmol per mouse, ip). BALB/c mice were treated with PGE_1 (50 μg/20 g bw, ip) 6, 9, or 12 h after the halothane administration. Twenty-four hours after the halothane administration, plasma IL-17 level was measured using ELISA. The data are means ± SD of three to five mice. Significantly different from halothane-administrated plus PGE_1-nontreated group (*$p < 0.05$).

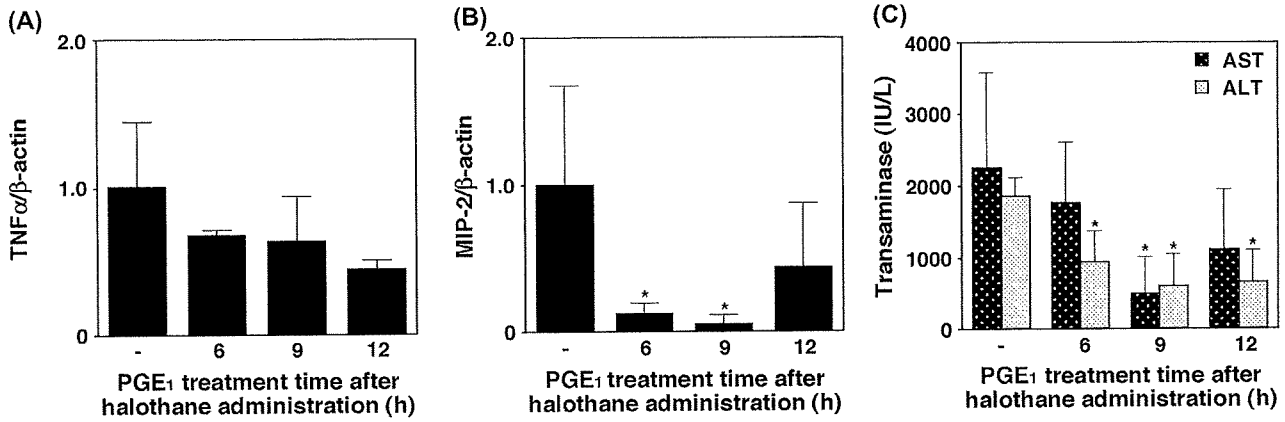

FIG. 6. Effect of PGE_1 treatment on hepatic mRNA expression in halothane-administrated BALB/c mice. Mice were administrated halothane (600 μmol per mouse, ip). Mice were treated with PGE_1 (50 μg/20g bw, ip) 6, 9, or 12 h after the halothane administration. Twenty-four hours after the halothane administration, hepatic mRNA expression was measured for TNF-α/β-actin (A), and MIP-2/β-actin (B) by real-time RT-PCR. Plasma for the AST and ALT assay were collected 24 h after the halothane administration (C). The data are means ± SD of three to four mice. Significantly different from halothane administrated plus PGE_1-nontreated group ($*p < 0.05$).

DISCUSSION

In this study, we investigated whether Th2-dominant BALB/c mice were more susceptible to halothane-induced liver injury than Th1-dominant C57BL/6 mice and whether MPO-positive cells had infiltrated in the hepatic centrilobular areas of halothane-administered BALB/c mice (Fig. 1). These results were consistent with those of previous studies in guinea pig (Lunam *et al.*, 1989) and mouse models (You *et al.*, 2006).

Previous studies have shown that T-bet and GATA-3 were Th1- and Th2-specific transcription factor, respectively (Szabo *et al.*, 2000; Zhang *et al.*, 1997). IFN-γ is a typical Th1 cytokine, and some studies suggested its involvement in T-cell–mediated liver injury and autoimmune disease (Kidd, 2003; Siebler *et al.*, 2003). IL-10 inhibits inflammatory cytokines (Glimcher and Murphy, 2000). Firstly, we investigated the relationship between halothane-induced liver injury and Th-cell–related factors. The hepatic T-bet/GATA-3 and IFN-γ/IL-10 mRNA expression ratios were decreased in susceptible BALB/c mice compared with C57BL/6 mice (Fig. 2). It was suggested that the mRNA expression ratio of T-bet/GATA-3 rather than the expression of either transcription factor alone reflected more closely the Th1/Th2 cytokine balance (Chakir *et al.*, 2003). The present observation suggested that the Th2 response would be driven in halothane-administered BALB/c mice and that a Th1/Th2 disbalance may be involved in halothane-induced liver injury as is the case for acetaminophen, lipopolysaccharide (LPS), and concanavalin A (Masubuchi *et al.*, 2008; Mizuhara *et al.*, 1998; Tanaka *et al.*, 1996). Although the increase of the hepatic mRNA expression of the proinflammatory mediator TNF-α was observed by halothane administration in both strains, we found that CXC chemokine MIP-2 mRNA expression was markedly increased only in BALB/c mice (Fig. 2). These results suggested that MIP-2 might be involved in halothane-induced liver injury.

IL-17, which is produced mainly by a specific subset of Th cells named Th17, stimulates the production of CXC chemokines (such as MIP-2 and keratinocyte-derived chemokine) and plays an important role in neutrophil activity (Zhu and Paul, 2008). Since the discovery of Th17, some immune-mediated diseases previously recognized as mediated by overactivation of the Th1-dominant response such as experimental autoimmune encephalomyelitis, collagen-induced arthritis, and inflammatory bowel disease, have now been suggested to be induced, at least in part, by Th17 cells (Zhu and Paul, 2008). It was demonstrated that IL-10 negatively regulates the expression of Th17 cytokines by both macrophages and T cells (Gu *et al.*, 2008). These lines of evidence prompted us to investigate the involvement of IL-17 in halothane-induced liver injury.

In the present study, we demonstrated that the plasma IL-17 level was increased by halothane administration in BALB/c mice, but not in C57BL/6 mice (Fig. 4), and neutralization of IL-17 significantly inhibited the increase of the plasma AST and ALT levels (Fig. 3C). In addition, the neutralization study demonstrated that the increase of MIP-2 expression in halothane-administered BALB/c mice was mediated by IL-17 (Fig. 3B). The administration of recombinant IL-17 caused a remarkable increase of the plasma AST and ALT levels (Fig. 4A) resulting in exacerbation of the hepatotoxic effect. From these lines of evidence, it is suggested that IL-17 is involved in the pathogenesis or exacerbation of halothane-induced liver injury. To the best of our knowledge, this is the first study demonstrating the involvement of IL-17 in drug-induced liver injury. The involvement of IL-17 in hepatotoxicity will be investigated in detail in the near future.

PGEs are known to protect against drug-induced liver injury or immune-mediated liver injury by downregulating the production of inflammatory cytokines. It was reported that the Th2-like response of liver T cells might be involved in the mechanism whereby PGE_1 protects against liver injury (Mokuno *et al.*, 1999). It has been demonstrated that PGE_1 inhibited superoxide production by neutrophils (Talpain *et al.*, 1995) and had a protective effect against carbon tetrachloride- and LPS-induced liver injury (Akamatsu *et al.*, 2001; Kayano *et al.*, 1995; Lindemann *et al.*, 2003; Mokuno *et al.*, 1999). However, no study has demonstrated the effect of PGE_1 on the plasma IL-17 level. These lines of reported data prompted us to investigate the effect of PGE_1 on the IL-17–related signaling in halothane-induced liver injury. In this study, the increased plasma IL-17 level, hepatic MIP-2 mRNA expression, and plasma AST and ALT levels in halothane-administrated BALB/c mice were inhibited by PGE_1 treatment (Figs. 5 and 6). Although many mechanisms of the protective effects of PGE_1 in liver injury have been elucidated, in the present study we found that inhibiting the IL-17 signal pathway could be one of the protective mechanisms of PGE_1 in halothane-induced liver injury.

A previous study suggested that p38 mitogen-activated protein kinase (MAPK) and NF-κB signaling pathway were activated in halothane-administered IL-10 deficient C57BL/6 mice (Feng *et al.*, 2009). In addition, the involvement of IL-17 in the p38 MAPK and nuclear factor kappa B (NF-κB)–signaling pathway was reported in human cardiac fibroblasts (Cortez *et al.*, 2007), and it was demonstrated that IL-10 negatively regulates the expression of Th17 cytokines and retinoid orphan receptor (RORγt) by both macrophages and T cells (Gu *et al.*, 2008). These reports supported the result of the present neutralization study.

Although the mechanism of drug-induced liver injury is still unclear due to the lack of animal models, LPS-treated rodents become sensitive to human hepatotoxic drugs, such as ranitidine, diclofenac, chlorpromazine, and trovafloxacin (Luyendyk *et al.*, 2003; Shaw *et al.*, 2009). LPS administration increased IL-17 in rodents (Ferretti *et al.*, 2003), but the involvement of IL-17 in the drug-induced liver injury in LPS-administered rodents was never reported. In addition to these LPS-drug models, mice deficient in IL-2– and suppressor of cytokine signaling (SOCS3-), which are negative regulators of the Th17-dominant response, were suggested to be useful for predicting human hepatotoxic drug candidates (Chen *et al.*, 2006; Romagnani, 2008). However, hepatic cytochrome P450s were markedly changed in a manner that was interleukin-concentration dependent (Siewert *et al.*, 2000). Especially, CYP2E1, the major enzyme of halothane metabolism, was down- or upregulated by various inflammatory cytokines (Hakkola *et al.*, 2003; Lagadic-Gossmann *et al.*, 2000), and Phase II detoxification abilities were lowered by interleukin (Romero *et al.*, 2002). Therefore, changes of the expression of drug metabolizing enzymes should be carefully pre-evaluated using IL-17 knockout mice.

The discovery of the Th17 T cell subset was a breakthrough that came from experimental autoimmune mice models (Romagnani, 2008). Although IL-17 has been recognized recently, a number of studies suggesting that IL-17 plays a critical function in autoimmune responses and protection against microbial challenges were already reported not only in mice but also in human. The present study supported the usefulness of the plasma IL-17 level for monitoring the severity of acute hepatic injury in human (Yasumi *et al.*, 2007).

In conclusion, we firstly reported that IL-17 determined the susceptibility against halothane-induced liver injury in mice. The marked increase of CXC chemokine MIP-2 and the increase of IL-17 in halothane-administered mice were investigated. Furthermore, PGE_1 treatment lowered the plasma IL-17 level and hepatic MIP-2 expression and protected against halothane-induced liver injury in mice. The present study sheds light on the mechanisms of drug-induced liver injury.

FUNDING

Health and Labor Sciences Research Grants from the Ministry of Health, Labor, and Welfare of Japan (H20-BIO-G001).

ACKNOWLEDGMENTS

We thank Mr Brent Bell for reviewing the manuscript.

REFERENCES

Akamatsu, K., Yamasaki, Y., Nishikawa, M., Takakura, Y., and Hashida, M. (2001). Synthesis and pharmacological activity of a novel water-soluble hepatocyte-specific polymeric prodrug of prostaglandin E_1 using lactosylated poly(L-glutamic hydrazide) as a carrier. *Biochem. Pharmacol.* **62,** 1531–1536.

Chakir, H., Wang, H., Lefebvre, D. E., Webb, J., and Scott, F. W. (2003). T-bet/GATA-3 ratio as a measure of the Th1/Th2 cytokine profile in mixed cell populations: Predominant role of GATA-3. *J. Immunol. Methods* **278,** 157–169.

Chen, Z., Laurence, A., Kanno, Y., Pacher-Zavisin, M., Zhu, B. M., Tato, C., Yoshimura, A., Henninghausen, L., and O'Shea, J. J. (2006). Selective regulatory function of Socs3 in the formation of IL-17-secreting T cells. *Proc. Natl. Acad. Sci. U. S. A.* **103,** 8137–8142.

Cortez, D. M., Feldman, M. D., Mummidi, S., Valente, A. J., Steffensen, B., Vincenti, M., Barnes, J. L., and Chandrasekar, B. (2007). IL-17 stimulates MMP-1 expression in primary human cardiac fibroblasts via p38 MAPK- and ERK1/2-dependent C/EBP-, NF-κB, and AP-1 activation. *Am. J. Physiol. Heart Circ. Physiol.* **293,** H3356–H3365.

Eliasson, E., Gardner, I., Hume-Smith, H., de Waziers, I., Beaune, P., and Kenna, J. G. (1998). Interindividual variability in P450-dependent generation of neoantigens in halothane hepatitis. *Chem. Biol. Interact.* **116,** 123–141.

Farrell, G. C., Frost, L., Tapner, M., Field, J., Weltman, M., and Mahoney, J. (1996). Halothane-induced liver injury in guinea-pigs: Importance of cytochrome P450 enzyme activity and hepatic blood flow. *J. Gastroenterol. Hepatol.* **11,** 594–601.

Feng, D., Wang, Y., Xu, Y., Luo, Q., Lan, B., and Xu, L. (2009). Interleukin 10 deficiency exacerbates halothane induced liver injury by increasing interleukin 8 expression and neutrophil infiltration. *Biochem. Pharmacol.* **77,** 277–284.

Ferretti, S., Bonneau, O., Dubois, G. R., Jones, C. E., and Trifilieff, A. (2003). IL-17, produced by lymphocytes and neutrophils, is necessary for lipopolysaccharide-induced airway neutrophilia: IL-15 as a possible trigger. *J. Immunol.* **170,** 2106–2112.

Fiorentino, D. F., Bond, M. W., and Mosmann, T. R. (1989). Two types of mouse T helper cell. IV. Th2 clone secrete a factor that inhibits cytokine production by Th1 clones. *J. Exp. Med.* **170,** 2081–2095.

Glimcher, L. H., and Murphy, K. M. (2000). Lineage commitment in the immune system: The T helper lymphocyte grows up. *Genes Dev.* **14,** 1693–1711.

Gu, Y., Yang, J., Ouyang, X., Liu, W., Li, H., Yang, J., Bromberg, J., Chen, S. H., Mayer, L., Unkeless, J. C., *et al.* (2008). Interleukin 10 suppresses Th17 cytokines secreted by macrophages and T cells. *Eur. J. Immunol.* **38,** 1807–1813.

Hakkola, J., Hu, Y., and Ingelman-Sundberg, M. (2003). Mechanisms of down-regulation of CYP2E1 expression by inflammatory cytokines in rat hepatome cell. *J. Pharmacol. Exp. Ther.* **304,** 1048–1054.

Holt, M. P., and Ju, C. (2006). Mechanisms of drug-induced liver injury. *AAPS J* **8,** E48–E54.

Kayano, K., Sakaida, I., Kubota, M., Yasunaga, M., and Okita, K. (1995). Functional differences between activated and normal rat liver macrophages: LPS uptake capacity by flow cytometric analysis in contrast with TNFα release. *Liver* **15,** 253–259.

Kidd, P. (2003). Th1/Th2 balance: The hypothesis, its limitations, and implications for health and disease. *Altern. Med. Rev.* **8,** 223–246.

Knight, B., Akhurst, B., Matthews, V. B., Ruddell, R. G., Ramm, G. A., Abraham, L. J., Olynyk, J. K., and Yeoh, G. C. (2007). Attenuated liver progenitor (oval) cell and fibrogenic responses to the choline deficient, ethionine supplemented diet in the BALB/c inbred strain of mice. *J. Hepatol.* **46,** 134–141.

Lagadic-Gossmann, D., Lerche, C., Rissel, M., Joannard, F., Galisteo, M., Guillouzo, A., and Corcos, L. (2000). The induction of the human hepatic CYP2E1 gene by interleukin 4 is transcriptional and regulated by protein kinase C. *Cell Biol. Toxicol.* **26,** 221–233.

Lind, R. C., Gandolfi, A. J., and Hall, P. D. (1989). Age and gender influence halothane-associated hepatotoxicity in strain 13 guinea pigs. *Anesthesiology* **71,** 878–884.

Lindemann, S., Gierer, C., and Darius, H. (2003). Prostacyclin inhibits adhesion of polymorphonuclear leukocytes to human vascular endothelial cells due to adhesion molecule independent regulatory mechanisms. *Basic Res. Cardiol.* **98,** 8–15.

Lunam, C. A., Hall, P. M., and Cousins, M. J. (1989). The pathology of halothane hepatotoxicity in a guinea-pig model: A comparison with human halothane hepatitis. *Br. J. Exp. Pathol.* **70,** 533–541.

Luyendyk, J. P., Maddox, J. F., Cosma, G. N., Ganey, P. E., Cockerell, G. L., and Roth, R. A. (2003). Ranitidine treatment during a modest inflammatory response precipitates idiosyncrasy-like liver injury in rats. *J. Pharmacol. Exp. Ther.* **307,** 9–16.

Masubuchi, Y., Sugiyama, S., and Horie, T. (2008). Th1/Th2 cytokine balance as a determinant of acetaminophen-induced liver injury. *Chem. Biol. Interact.* **179,** 273–279.

Mizuhara, H., Kuno, M., Seki, N., Yu, W. G., Yamaoka, M., Yamashita, M., Ogawa, T., Kaneda, K., Fujii, T., Senoh, H., *et al.* (1998). Strain difference in the induction of T-cell activation-associated, interferon gamma-dependent hepatic injury in mice. *Hepatology* **27,** 513–519.

Mokuno, Y., Takano, M., Matsuguchi, T., Nishimura, H., Washizu, J., Naiki, Y., Nimura, Y., and Yoshikai, Y. (1999). Prostaglandin E_1 protects against liver injury induced by *Escherichia coli* infection via a dominant Th2-like response of liver T cells in mice. *Hepatology* **30,** 1464–1472.

Ramaiah, S. K., and Jaeschke, H. (2007). Role of neutrophils in the pathogenesis of acute inflammatory liver injury. *Toxicol. Pathol.* **35,** 757–766.

Ray, D. C., and Drummond, G. B. (1991). Halothane hepatitis. *Br. J. Anaesthesiol.* **67,** 84–99.

Romagnani, S. (2008). Human Th17 cells. *Arthritis Res. Ther.* **10,** 206.

Romero, L., Higgins, M. A., Gilmore, J., Boudreau, K., Maslen, A., Barker, H. J., and Kirby, G. M. (2002). Down-regulation of alpha class glutathione S-transferase by interleukin-1beta in human intestinal epithelial cells (Caco-2) in culture. *Drug Metab. Dispos.* **30,** 1186–1193.

Shaw, P. J., Ditewig, A. C., Waring, J. F., Liguori, M. J., Blomme, E. A., Ganey, P. E., and Roth, R. A. (2009). Coexposure of mice to trovafloxacin and lipopolysaccharide, a model of idiosyncratic hepatotoxicity, results in a unique gene expression profile and interferon γ-dependent liver injury. *Toxicol. Sci.* **107,** 270–280.

Siebler, J., Wirtz, S., Klein, S., Protschka, M., Blessing, M., Galle, P. R., and Neurath, M. F. (2003). A key pathogenic role for the STAT1/T-bet signaling pathway in T-cell-mediated liver inflammation. *Hepatology* **38,** 1573–1580.

Siewert, E., Bort, R., Kluge, R., Heinrich, P. C., Castell, J., and Jover, R. (2000). Hepatic cytochrome P450 down-regulation during aseptic inflammation in the mouse is interleukin 6 dependent. *Hepatology* **32,** 49–55.

Szabo, S. J., Kim, S. T., Costa, G. L., Zhang, X., Fathman, C. G., and Glimcher, L. H. (2000). A novel transcription factor, T-bet, directs Th1 lineage commitment. *Cell* **100,** 655–669.

Talpain, E., Armstrong, R. A., Coleman, R. A., and Vardey, C. J. (1995). Characterization of the PGE receptor subtype mediating inhibition of superoxide production in human neutrophils. *Br. J. Pharmacol.* **114,** 1459–1465.

Tanaka, Y., Takahashi, A., Watanabe, K., Takayama, K., Yahata, T., Habu, S., and Nishimura, T. (1996). A pivotal role of IL-12 in Th1-dependent mouse liver injury. *Int. Immunol.* **8,** 569–576.

Yasumi, Y., Takikawa, Y., Endo, R., and Suzuki, K. (2007). Interleukin-17 as a new marker of severity of acute hepatic injury. *Hepatol. Res.* **37,** 248–254.

You, Q., Cheng, L., Reilly, T. P., Wegmann, D., and Ju, C. (2006). Role of neutrophils in a mouse model of halothane-induced liver injury. *Hepatology* **44,** 1421–1431.

Zhang, D. H., Cohn, L., Ray, P., Bottomly, K., and Ray, A. (1997). Transcription factor GATA-3 is differentially expressed in murine Th1 and Th2 cells and controls Th2-specific expression of the interleukin-5 gene. *J. Biol. Chem.* **272,** 21597–21603.

Zhu, J., and Paul, W. E. (2008). CD4 T cells: Fates, functions, and faults. *Blood* **112,** 1557–1569.

0026-895X/09/7604-702–709$20.00
MOLECULAR PHARMACOLOGY
Copyright © 2009 The American Society for Pharmacology and Experimental Therapeutics
Mol Pharmacol 76:702–709, 2009

Vol. 76, No. 4
56986/3511093
Printed in U.S.A.

Human CYP24 Catalyzing the Inactivation of Calcitriol Is Post-Transcriptionally Regulated by miR-125b

Sayaka Komagata, Miki Nakajima, Shingo Takagi, Takuya Mohri, Takao Taniya, and Tsuyoshi Yokoi

Drug Metabolism and Toxicology, Faculty of Pharmaceutical Sciences, Kanazawa University, Kanazawa, Japan (S.K., M.N., S.T., T.M., T.Y.); and Futaba Breast Clinic, Kanazawa, Japan (T.T.)

Received April 10, 2009; accepted July 1, 2009

ABSTRACT

Human vitamin D_3 hydroxylase (CYP24) catalyzes the inactivation of 1α,25-dihydroxyvitamin D_3 (calcitriol), which exerts antiproliferative effects. CYP24 has been reported to be overexpressed in various cancers in which microRNA levels are dysregulated. In silico analysis identified a potential miR-125b recognition element (MRE125b) in the 3′-untranslated region of human CYP24 mRNA. We investigated whether CYP24 is regulated by miR-125b. In luciferase assays using a reporter plasmid containing MRE125b, transfection of the antisense oligonucleotide (AsO) for miR-125b increased the reporter activity in KGN cells, and transfection of precursor miR-125b decreased the reporter activity in MCF-7 cells. The endogenous CYP24 protein level was also increased by AsO for miR-125b in KGN cells and was decreased by precursor miR-125b in MCF-7 cells. These results suggested that human CYP24 is regulated by miR-125b. Immunohistochemical analysis revealed that the CYP24 protein levels in human breast cancer were higher than in adjacent normal tissues, without an accompanying CYP24 mRNA increase. On the other hand, the expression levels of miR-125b in cancer tissues were significantly ($P < 0.0005$) lower than those in normal tissues. It is noteworthy that the CYP24 protein levels in cancer tissues were inversely associated with the cancer/normal ratios of the miR-125b levels, indicating that the decreased miR-125b levels in breast cancer tissues would be one of the causes of the high CYP24 protein expression. In conclusion, this study clearly demonstrates that miR-125b post-transcriptionally regulates the CYP24, which serves as a possible mechanism for the high CYP24 expression in cancer tissues.

Human CYP24 is a key enzyme involved in the inactivation of 1α,25-dihydroxyvitamin D_3 [1,25$(OH)_2D_3$; calcitriol]. 1,25$(OH)_2D_3$ is typically considered a regulator of calcium homeostasis, but it has now received much interest for its antitumor activity (Deeb et al., 2007). For ensuring the appropriate biological effects of 1,25$(OH)_2D_3$, the balance between bioactivation and inactivation is critical. CYP24 has been reported to be overexpressed in various tumor cells (Deeb et al., 2007). Because CYP24 limits the biological activity of the vitamin D signaling system, the overexpression may abrogate the vitamin D-mediated growth control. In fact, it has been reported that the overexpression of CYP24 is associated with poor prognosis and overall reduced survival in patients with esophageal cancer (Mimori et al., 2004). As for the cause of the CYP24 overexpression, an amplification of the chromosomal region 20q13.2, where the *CYP24* gene is located, in human breast cancer was reported (Kallioniemi et al., 1994; Albertson et al., 2000). Albertson et al. (2000) found that the relative levels of CYP24 mRNA were higher in breast cancers with the amplification, although the number of samples was only three. Townsend et al. (2005) also reported increased CYP24 mRNA levels in breast cancers. On the other hand, de Lyra et al. (2006) reported that there was no difference in the CYP24 mRNA levels between breast cancer and normal tissues. In contrast, Anderson et al. (2006) reported that CYP24 mRNA was down-regulated in breast cancer relative to normal tissues. Although we cannot compare these expression profiles because the genetic background is heterogeneous in different breast cancer cells (Hicks et al., 2006), the overexpression of CYP24 protein is not necessarily associated with the increased CYP24 mRNA level. This background allowed us to postulate the

This work was supported in part by Research on Advanced Medical Technology, Health, and Labor Science Research from the Ministry of Health, Labor, and Welfare of Japan [Grant H20-BIO-G001] and by the Takeda Sciences Foundation.
Article, publication date, and citation information can be found at http://molpharm.aspetjournals.org.
doi:10.1124/mol.109.056986.

ABBREVIATIONS: miRNA, microRNA; 1,25$(OH)_2D_3$, 1α,25-dihydroxyvitamin D_3; MRE125b, miR-125b recognition element; AsO, antisense oligonucleotide; UTR, untranslated region; HEK, human embryonic kidney; DMEM, Dulbecco's modified Eagle's medium; FBS, fetal bovine serum; RT-PCR, reverse transcription-polymerase chain reaction; VDR, vitamin D receptor; GAPDH, glyceraldehyde-3-phosphate dehydrogenase.

involvement of a post-transcriptional mechanism in CYP24 regulation.

MicroRNAs (miRNAs) are endogenous ~22-nucleotide noncoding RNAs that regulate gene expression through the translational repression or degradation of target mRNAs (Bartel, 2004). The human genome may contain up to 1000 miRNAs, and 30% of human mRNAs are predicted to be targets of miRNAs (Lewis et al., 2005). Accumulating evidence has revealed an important role of miRNAs in cancer (Medina and Slack, 2008). In various cancers, the miRNA levels are dysregulated (Lu et al., 2005). In the present study, we investigated whether miRNAs may be involved in the regulation of the human CYP24 expression.

Materials and Methods

Chemicals and Reagents. $1,25(OH)_2D_3$ and corticosterone were purchased from Wako Pure Chemical Industries (Osaka, Japan). $25(OH)D_3$ and $24,25(OH)_2D_3$ were from Funakoshi (Tokyo, Japan). The pGL3-promoter vector, phRL-TK plasmid, Tfx-20 reagent, and a dual-luciferase reporter assay system were purchased from Promega (Madison, WI). LipofectAMINE 2000 and LipofectAMINE RNAiMAX were from Invitrogen (Carlsbad, CA). PremiR miRNA precursors for miR-125b-1 and negative control 2 were from Ambion (Austin, TX). Antisense locked nucleic acid/DNA mixed oligonucleotides (AsO) for miR-125b (5′-TCACAAGTTAGGGTCTCAGGGA-3′, underlined letters show locked nucleic acid) and for negative control (5′-AGACTAGCGGTATCTTAAACC-3′) were from Greiner Japan (Tokyo, Japan). All primers and oligonucleotides were commercially synthesized at Hokkaido System Sciences (Sapporo, Japan). Goat anti-human CYP24 polyclonal antibodies and Alexa Fluor 680 donkey anti-goat IgG were from Santa Cruz Biotechnology (Santa Cruz, CA) and Invitrogen, respectively. All other chemicals and solvents were of the highest grade available commercially.

Cells and Culture Conditions. The human breast adenocarcinoma cell lines MCF-7 and MDA-MB-435 and the human embryonic kidney (HEK) cell line 293 were obtained from the American Type Culture Collection (Manassas, VA). The human ovarian granulosa-like tumor cell line KGN (Nishi et al., 2001) and the human hepatoma cell line HepG2 were obtained from Riken Gene Bank (Tsukuba, Japan). MCF-7 cells were cultured in Dulbecco's modified Eagle's medium (DMEM; Nissui Pharmaceutical, Tokyo, Japan) supplemented with 0.1 mM nonessential amino acid (Invitrogen) and 10% fetal bovine serum (FBS; Invitrogen). MDA-MB-435 cells and HepG2 cells were cultured in DMEM supplemented with 10% FBS. HEK293 cells were cultured in DMEM supplemented with 4.5 g/l glucose, 10 mM HEPES, and 10% FBS. KGN cells were cultured in a 1:1 mixture of DMEM and Ham's F-12 medium (Nissui Pharmaceutical) supplemented with 10% FBS. These cells were maintained at 37°C under an atmosphere of 5% CO_2/95% air.

Northern Blot Analysis and Real-Time RT-PCR for Mature miR-125b. Total RNA (20 μg) isolated from the cells using ISOGEN (Nippon Gene, Tokyo, Japan) was separated on 15% denaturing polyacrylamide gels containing 8 M urea. The RNA was then electrophoretically transferred to Zeta-Probe GT Genomic Tested Blotting Membranes (Bio-Rad Laboratories, Hercules, CA). The membranes were probed with ^{32}P-labeled DNA probe for miR-125b (5′-TCA CAA GTT AGG GTC TCA GGG A-3′), and then the miRNAs were detected and quantified with a Fuji Bio-Imaging Analyzer BAS 1000 (Fuji Film, Tokyo, Japan).

For quantification of mature miR-125b, polyadenylation and reverse transcription were performed using an NCode miRNA First-Strand cDNA Synthesis Kit (Invitrogen) according to the manufacturer's protocol. The forward primer for miR-125b was 5′-TCC CTG AGA CCC TAA CTT GTG A-3′, and the reverse primer was the supplemented universal quantitative polymerase chain reaction primer. The real-time polymerase chain reaction was performed using the Smart Cycler (Cepheid, Sunnyvale, CA) with Smart Cycler software (version 1.2b) as follows: after an initial denaturation at 95°C for 30 s, the amplification was performed by denaturation at 95°C for 10 s and annealing and extension at 60°C for 10 s for 45 cycles.

SDS-Polyacrylamide Gel Electrophoresis and Western Blot Analyses for CYP24 Protein and Real-Time RT-PCR for CYP24 mRNA. Whole-cell lysates were prepared by homogenization with lysis buffer (50 mM Tris-HCl, pH 8.0, 150 mM NaCl, 1 mM EDTA, and 1% Nonidet P-40) containing protease inhibitors (0.5 mM *p*-amidinophenyl methanesulfonyl fluoride hydrochloride, 2 μg/ml aprotinin, and 2 μg/ml leupeptin). The protein concentrations were determined using Bradford protein assay reagent (Bio-Rad). The whole-cell lysates (20 μg) were separated by 10% SDS-polyacrylamide gel electrophoresis and transferred to Immobilon-P transfer membrane (Millipore Corporation, Billerica, MA). The membrane was probed with goat anti-human CYP24 antibodies and Alexa Fluor 680 donkey anti-goat IgG antibodies. The band densities were quantified using the Odyssey Infrared Imaging System (LI-COR Biosciences, Cambridge, UK).

The cDNAs were synthesized from total RNAs using ReverTra Ace (Toyobo, Osaka, Japan). The forward and reverse primers for CYP24 mRNA were 5′-CAG CAA ACA GTC TAA TGT GG-3′ and 5′-AGC ATA TTC ACC CAG AAC TG-3′, respectively. The real-time RT-PCR analysis was performed as follows: after an initial denaturation at 95°C for 30 s, the amplification was performed by denaturation at 94°C for 4 s and annealing and extension at 62°C for 20 s for 45 cycles. The CYP24 mRNA levels were normalized with GAPDH mRNA determined by real-time RT-PCR as described previously (Tsuchiya et al., 2004).

Construction of Reporter Plasmids. To construct luciferase reporter plasmids, various target fragments were inserted into the XbaI site, downstream of the luciferase gene in the pGL3-promoter vector. The sequence from +1575 to +1592 in the human *CYP24* gene (5′-TCA TAT CCA ACT CAG GGA-3′) was termed miR-125b recognition element (MRE125b). The fragment containing three copies of the MRE125b, 5′-CTA GAT TTG CTA ACA TCA TAT CCA ACT CAG GGA AGC GGA TTT GCT AAC ATC ATA TCC AAC TCA GGG AAG CGG ATT TGC TAA CAT CAT ATC CAA CTC AGG GAA GCG GAT-3′ (MRE125b is underlined), was cloned into the pGL3-promoter vector (pGL3/MRE3). The complementary sequence was also cloned into the pGL3-promoter vector (pGL3/MRE3rev). A fragment containing the perfect matching sequence with the mature miR-125b, 5′-CTA GAT CAC AAG TTA GGG TCT CAG GGA T-3′ (the matching sequence is underlined), was cloned (pGL3/c-miR-125b). A fragment containing the sequence from +1529 to +1609 was cloned, resulting in single (pGL3/UTR1) and double (pGL3/UTR2) forward insertions and a single reverse insertion (pGL3/UTR1rev). The nucleotide sequences of the constructed plasmids were confirmed by DNA sequencing analyses.

Luciferase Assay. Various pGL3 plasmids were transiently transfected with phRL-TK plasmid into KGN and MCF-7 cells. In

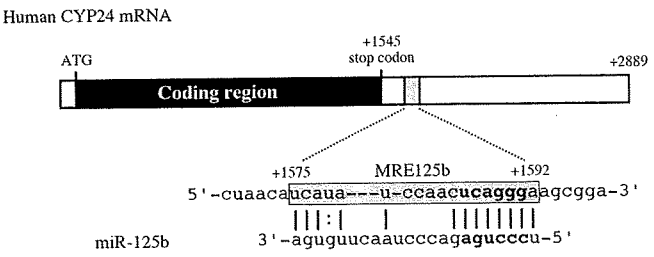

Fig. 1. Predicted target sequence of miR-125b in the human CYP24 mRNA. The numbering refers to the ATG in translation starting with A as 1, and the coding region is up to +1545. Sequence of MRE125b (gray box) is located on +1575 to +1592 in the 3′-UTR of human CYP24 mRNA. Boldface letters represent seed sequence.

brief, the day before transfection, the KGN cells (8×10^4 cells/well) and MCF-7 cells (4×10^4 cells/well) were seeded into 24-well plates. After 24 h, 450 ng of pGL3 plasmid and 50 ng of phRL-TK plasmid were transfected using Tfx-20 reagent. To KGN cells, 3.5 pmol of AsOs for miR-125b or control was cotransfected using LipofectAMINE 2000; to MCF-7 cells, 0.25 pmol of precursors for miR-125b-1 or control was cotransfected using Tfx-20 reagent. After incubation for 48 h, the cells were resuspended in passive lysis buffer, and then the luciferase activity was measured with a Wallac luminometer (PerkinElmer Life and Analytical Sciences, Turku Finland) using the dual-luciferase reporter assay system.

Assessment of the Endogenous CYP24 Expression Level in KGN and MCF-7 Cells. To investigate the effects of miR-125b on the expression of endogenous CYP24 protein, 50 nM precursors or 50 nM AsOs for miR-125b or control were transfected into KGN (4×10^5 cells/well) and MCF-7 cells (2.5×10^5 cells/well), respectively, on six-well plates using LipofectAMINE RNAiMAX. After 72 h, total RNA was isolated using ISOGEN, and the mature miR-125b levels were determined by Northern blot analysis. Whole-cell lysate was prepared, and the CYP24 protein level was determined by Western blot analysis. The CYP24 protein levels were normalized with the β-actin protein levels determined with rabbit anti-human β-actin antibodies (BioVision, Mountain View, CA) and IRDye 680 goat anti-rabbit IgG antibodies (LI-COR Biosciences). To determine the CYP24 enzymatic activity, $24,25(OH)_2D_3$ formation from $25(OH)D_3$ was measured. The KGN and MCF-7 cells seeded on six-well plates were transfected with AsO and precursor as described above. After 24 h, the cells were treated with 50 nM $1,25(OH)_2D_3$ for 24 h to induce CYP24 expression. The cells were then incubated with $25(OH)D_3$ in the medium supplemented with 3% FBS for 18 h. To the collected medium, corticosterone was added as an internal standard. The medium was extracted with 4 volumes of chloroform/methanol (3:1). The organic phase was recovered and dried. The resulting residue was dissolved with 50% acetonitrile and was subjected to high-performance liquid chromatography. The column used was an YMC-Pack ODS-A (6.0 × 300 mm, 5 μm) column (YMC, Tokyo, Japan), and the column temperature was 35°C. The mobile phase was 55% acetonitrile containing 0.2% acetic acid (A) and 90% acetonitrile (B). The condition for elution was as follows: 0% B (0–40 min); 0 to 100% B (40–50 min); 100% B (50–60 min); and 100 to 0% B (60–65 min). Linear gradients were used for all solvent changes. The flow rate was 1.0 ml/min. The eluent was monitored at 265 nm. The retention times of corticosterone, $24,25(OH)_2D_3$, and $25(OH)D_3$ were 9, 41, and 61 min, respectively. The quantification of the metabolite was performed by comparing the high-performance liquid chromatography peak height with that of an authentic standard with reference to the internal standard.

Human Breast Cancer and Adjacent Normal Tissues. This study was approved by the Ethics Committee of Kanazawa University (Kanazawa, Japan). Written informed consent was obtained from patients before their participation in this study. Breast cancer and adjacent normal tissues were obtained as surgical samples from 14 Japanese patients with primary breast carcinoma. The patients (42–77 years old) had not undergone chemotherapy. Thirteen patients with invasive ductal carcinoma and one patient with invasive lobular carcinoma were participants. The histological grade was determined by standard criteria as grade 1–2 ($n = 9$), grade 2 ($n = 4$), and grade 2–3 ($n = 1$). The samples were obtained immediately after resection, divided into breast cancer and adjacent normal tissues, and immediately frozen with liquid nitrogen. The samples were stored at −80°C until use. The expression levels of mature miR-125b were determined by real-time RT-PCR and were normalized with the

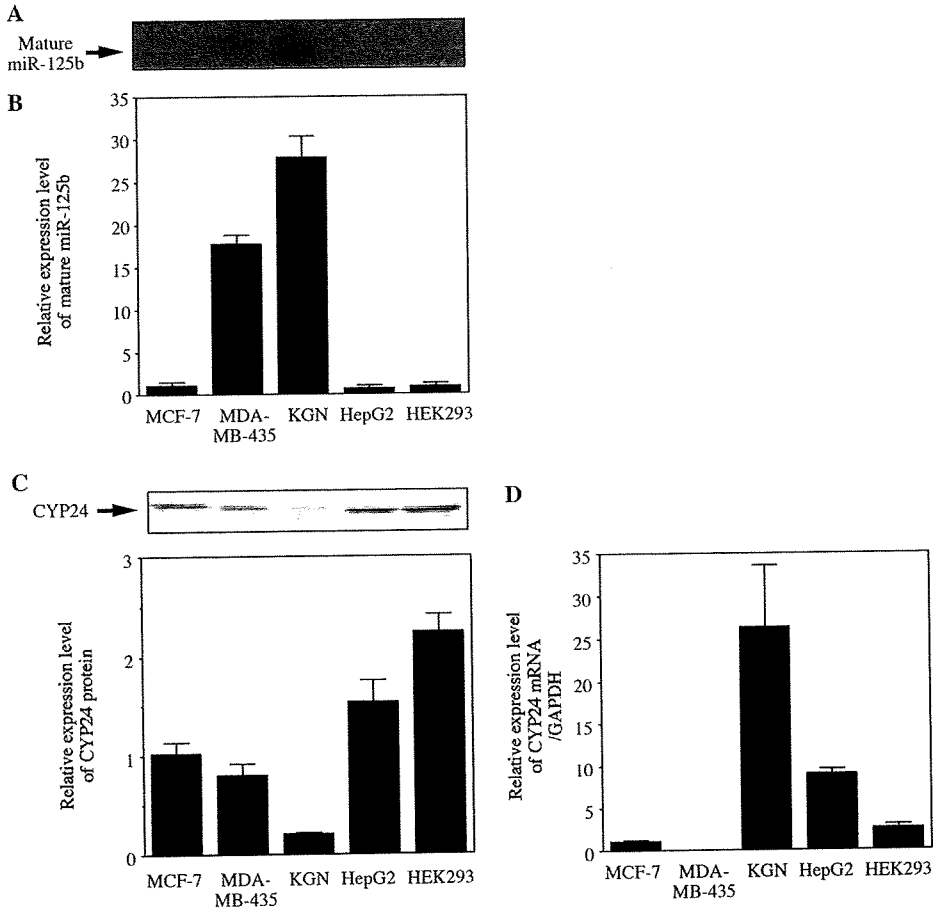

Fig. 2. Expression levels of miR-125b and CYP24 in various human cell lines. A, the expression levels of mature miR-125b in MCF-7, MDA-MB-435, KGN, HepG2, and HEK293 cells were determined by Northern blot analyses. B, the expression levels of mature miR-125b were determined by real-time RT-PCR. C, the expression levels of CYP24 protein were determined by Western blot analyses. D, the expression levels of CYP24 mRNA were determined by real-time RT-PCR. The expression levels were normalized with the expression level of GAPDH as a control. Values are expressed relative to the values in MCF-7 cells. Data are the mean ± S.D. of triplicate determinations.

18S rRNA levels determined by real-time RT-PCR as follows: the forward and reverse primers were 5′-GGC CCT GTA ATT GGA ATG AGT C-3′ and 5′-GAC ACT CAG CTA AGA GCA TCG-3′, respectively. After an initial denaturation at 95°C for 30 s, the amplification was performed by denaturation at 94°C for 10 s, with annealing and extension at 68°C for 20 s for 30 cycles.

Immunohistochemistry. Immunohistochemical analyses of CYP24 were performed using formalin-fixed, paraffin-embedded specimens of breast cancer tissues from 14 patients. The sections were soaked in Liberate Antibody Binding Solution (Polysciences, Warrington, PA) at room temperature for 10 min and then incubated with anti-human CYP24 antibodies at 4°C for 16 h. Staining was performed using a VECTASTAIN ABC kit (Vector Laboratories, Burlingame, CA). The extent of immunostaining in cancer cells was evaluated by the intensity of staining, dividing the samples into three groups (low, medium, and high levels).

Statistical Analyses. Data are expressed as mean ± S.D. of triplicate determinations or three independent experiments. Statistical significance was determined by analysis of variance and Dunnett's multiple comparisons test. Comparison of two groups was made with an unpaired, two-tailed Student's t test. Correlation analysis was performed by Spearman's rank method. The statistical significance of difference between the expression level of miR-125b in breast cancer and normal tissues was determined by paired, two-tailed Student's t test. The relationship between the CYP24 protein level and the cancer/normal ratio in miR-125b level was investigated by analysis of variance and Tukey method test. A value of $P < 0.05$ was considered statistically significant.

Results

miR-125b Interacts with the 3′-UTR of Human CYP24 mRNA. Computational predictions using the microRNA targets web site (http://www.targetscan.org/) indicate that miR-125b shares complementarity with a sequence in the 3′-UTR of the CYP24 mRNA at +1575 to +1592 (energy, −21.6 kcal/mol) (Fig. 1). This region was termed the miR-125b recognition element (MRE125b). The seed sequence (nucleotides 2–7) of miR-125b was perfectly matched with the predicted binding site of the CYP24 mRNA. In this study, we investigated whether miR-125b might be involved in the regulation of human CYP24 expression through the MRE125b.

miR-125b and CYP24 Are Differentially Expressed in Human Cell Lines. The expression levels of mature miR-125b in MCF-7, MDA-MB-435, KGN, HepG2, and HEK293 cells were determined by Northern blot analysis. KGN and MDA-MB-435 cells showed a clear band of mature miR-125b, but the other cell lines did not (Fig. 2A). We also performed real-time RT-PCR analysis using NCode miRNA First-Strand cDNA Synthesis Kit (Fig. 2B) to detect the mature miR-125b because this method is more sensitive than Northern blot analysis. Extremely low levels of the mature miR-125b were detected in MCF-7, HepG2, and HEK293 cells. The CYP24 protein levels were determined by Western blot analyses (Fig. 2C), and the CYP24 mRNA levels were determined by real-time RT-PCR (Fig. 2D). The CYP24 protein levels were not positively correlated ($R_s = -0.100, P = 0.950$) with the CYP24 mRNA levels, indicating the post-transcriptional regulation of CYP24. It is noteworthy that a trend of inverse association between the CYP24 protein levels and the mature miR-125b levels was found ($R_s = -0.900, P = 0.083$).

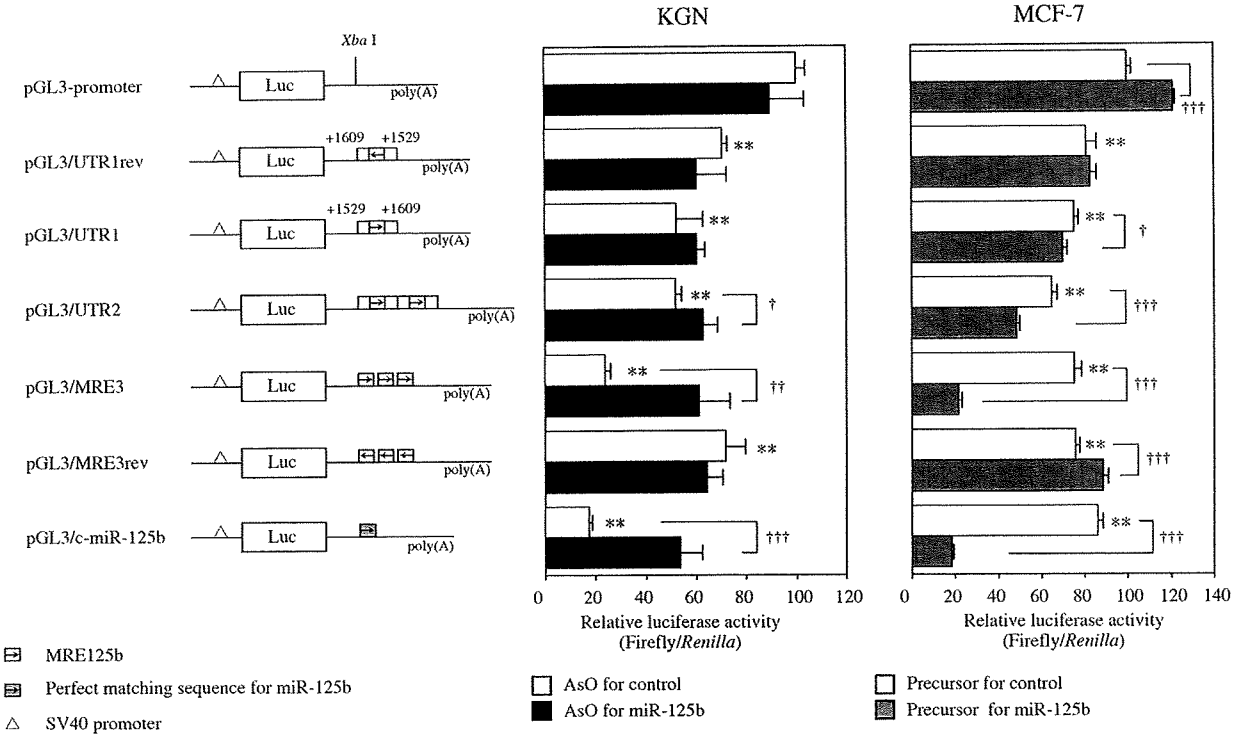

Fig. 3. Luciferase assays with reporter constructs containing MRE125b in human CYP24 in KGN and MCF-7 cells. A series of reporter constructs containing the 3′-UTR of the human CYP24 was transiently transfected into KGN cells with the AsO for miR-125b or control, or into MCF-7 cells with the precursors for miR-125b or control. The firefly luciferase activity for each construct was normalized with the *Renilla reniformis* luciferase activities. Values are expressed as percentages of the relative luciferase activity of pGL3-promoter plasmid. Each column represents the mean ± S.D. of three independent experiments. **, $P < 0.01$, compared with pGL3-promoter by analysis of variance and Dunnett test. †, $P < 0.05$; ††, $P < 0.01$; †††, $P < 0.005$ compared with the control by Student's t test.

MRE125b in CYP24 Is a Target of Post-Transcriptional Repression by miR-125b. To investigate whether MRE125b is functional in the regulation by miR-125b, luciferase assays were performed. The pGL3/MRE3 plasmid containing three copies of the MRE125b was used because it is known that the multiplicity of the binding site allows efficacious detection of the effects of miRNA. The pGL3/UTR1 plasmid was used to investigate whether the intact 3′-UTR sequence of CYP24, including MRE125b, can be recognized by miRNA. The pGL3/UTR2 plasmid was used to confirm whether the multiplicity could intensify the effects of miRNA. The pGL3/c-miR-125b plasmid containing the perfect matching sequence with the mature miR-125b was used as a positive control. These plasmids were transfected into the KGN cells showing the highest expression of miR-125b (Fig. 2A). We first confirmed that the luciferase activity of the pGL3/c-miR-125b plasmid was significantly ($P < 0.01$) lower than that of the control pGL3-promoter and was significantly ($P < 0.005$) restored by the transfection of AsO for miR-125b (Fig. 3). The reporter activity of the pGL3/MRE3 plasmid was also significantly lower than that of the control plasmid, and it was significantly ($P < 0.01$) restored by the transfection of AsO for miR-125b. The reporter activities of the pGL3/UTR1 and pGL3/UTR2 were also significantly lower than that of the control plasmid, and the activity of pGL3/UTR2 was significantly ($P < 0.05$) restored by the transfection of AsO for miR-125b. Next, to investigate the effect of the overexpression of miR-125b on the luciferase activity, the precursor for miR-125b was transfected in MCF-7 cells in which the endogenous miR-125b level was low. The overexpression of miR-125b significantly decreased the luciferase activities of the pGL3/c-miR-125b, pGL3/MRE3, pGL3/UTR1, and pGL3/UTR2 plasmids. These results suggest that miR-125b recognized the MRE125b on the human CYP24 mRNA and regulated the expression.

Endogenous CYP24 Levels Are Regulated by miR-125b. We investigated the effects of inhibition of miR-125b on the CYP24 protein level and enzymatic activity in KGN cells. Northern blot analysis confirmed that the endogenous miR-125b level was prominently decreased by the transfection of the AsO for miR-125b (Fig. 4A). As shown in Fig. 4B, the CYP24 protein level was significantly ($P < 0.005$) increased (1.4-fold) by the transfection of the AsO for miR-125b. The 25(OH)D_3 24-hydroxylase activity was also increased by the transfection of the AsO, although the difference was statistically insignificant (Fig. 4C). We next investigated the effects of overexpression of miR-125b on the CYP24 protein level and enzymatic activity in MCF-7 cells. Northern blot analysis confirmed that the mature miR-125b level was prominently increased by the transfection of the precursor for miR-125b (Fig. 4A). As shown in Fig. 4B, the CYP24 protein level was significantly ($P < 0.05$) decreased (70% of control) by the transfection of the precursor for miR-125b. The 25(OH)D_3 24-hydroxylase activity was also significantly ($P < 0.05$) decreased by the transfection of the precursor (Fig. 4C). These results suggest that miR-125b regulates the endogenous CYP24 level.

CYP24 Protein Levels Are Inversely Associated with miR-125b Levels in Human Breast Cancer. To investigate whether miR-125b affects the CYP24 expression in vivo, we used breast cancer tissues from 14 patients. The expression levels of CYP24 protein in breast cancer were determined by immunohistochemistry (Fig. 5A). All of the breast tissues showed cytoplasmic immunoreactivity for CYP24. The CYP24 protein levels were higher in cancer tissues than in adjacent normal tissues. The extent of CYP24 staining in cancer tissues varied among individuals. No staining was observed in normal goat IgG. In regard to the CYP24 mRNA, the levels normalized with GAPDH mRNA were lower in cancer tissues than in normal tissues (data not shown). This was due to the increased levels of GAPDH mRNA in the cancer tissues. When the non-normalized CYP24 mRNA levels in the cancer and normal tissues were compared, there was no difference. In addition, no difference was observed in

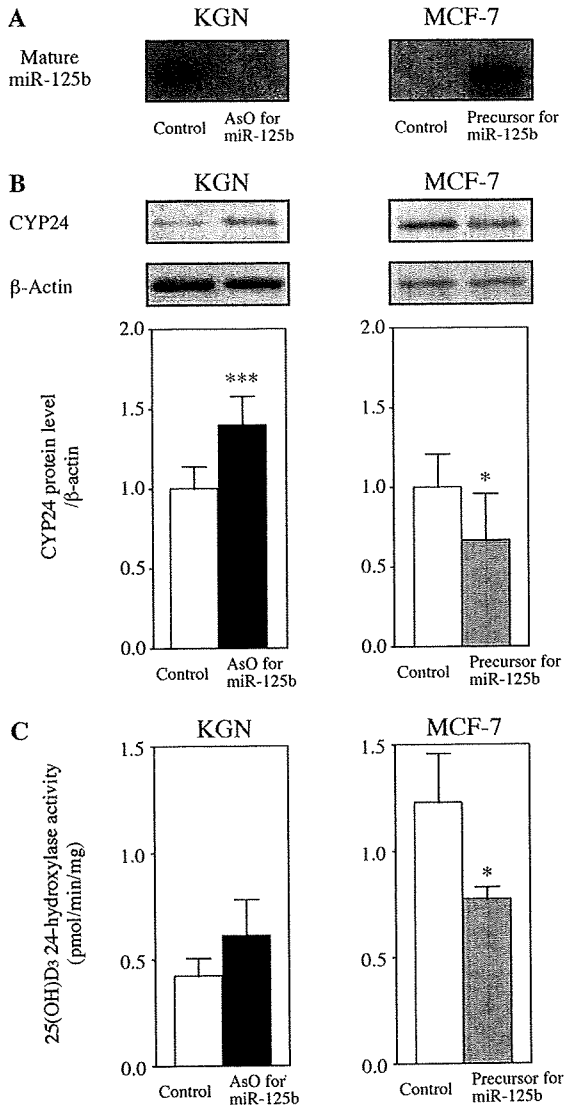

Fig. 4. Effects of miR-125b on the endogenous CYP24 protein level in KGN or MCF-7 cells. AsOs for miR-125b or control (2.5 pmol/4 × 10^5 cells) were transfected into KGN cells and precursors for miR-125b or control (84 pmol/1.68 × 10^5 cells) were transfected into MCF-7 cells. After 72 h, total RNA and whole-cell lysate were prepared. A, the expression levels of mature miR-125b were determined by Northern blot analysis. B, the expression levels of CYP24 protein were determined by Western blot analysis. C, the CYP24 enzymatic activity was determined using 25(OH)D_3 as a substrate as described under *Materials and Methods*. Each column represents the mean ± S.D. of three independent experiments. *, $P < 0.05$; ***, $P < 0.005$ compared with the control.

the CYP24 mRNA levels normalized with the 18S rRNA levels in the cancer and normal tissues (data not shown). Thus, the higher levels of CYP24 protein in cancer tissues would not be due to the increased CYP24 mRNA levels. As shown in Fig. 5B, the mature miR-125b levels normalized with the 18S rRNA levels in the cancer tissues were significantly ($P < 0.0005$) lower than those in normal tissues, in agreement with previous studies (Calin et al., 2004; Iorio et al., 2005). It is noteworthy that an inverse association was observed between the CYP24 protein levels in breast cancer tissue and the cancer/normal ratio of mature miR-125b levels (Fig. 5C). These results suggest that the decrease of miR-125b is one of the causes of the high expression of CYP24 protein in breast cancer tissues. No association was observed between the levels of CYP24 or miR-125b and the biopathological features (estrogen receptor and progesterone receptor levels and the presence or absence of lymph node metastasis) and the tumor stage of breast cancer (data not shown). Thus, the pathological characteristics would not affect the inverse association between the CYP24 and miR-125b levels.

Discussion

In the present study, we investigated whether human CYP24, which catalyzes the inactivation of $1,25(OH)_2D_3$, might be a target of miRNA. In silico analysis identified MRE125b in the 3′-UTR in CYP24 mRNA. The luciferase assay revealed that the endogenous and exogenous miR-125b negatively regulated the activity through MRE125b. Consistent with previous reports (Tsuchiya et al., 2006; Wang et al., 2006), the repression was increased by multiplicity of the binding site. The AsO for miR-125b restored the luciferase activity. These results suggest that the MRE125b is functionally recognized by miR-125b. The overall complementarity of MRE125b for miR-125b is low, but the seed sequence of miR-125b was perfectly matching. Therefore, the seed-sequence matching and accessibility of CYP24 would allow access to miR-125b. Furthermore, the endogenous CYP24 protein level was increased by the inhibition of miR-125b and was decreased by the overexpression of miR-125b. These results clearly indicate that human CYP24 is post-transcriptionally regulated by miR-125b.

It has been reported that human CYP24 is regulated by transcription factors such as vitamin D receptor (VDR) (Chen and DeLuca, 1995), pregnane X receptor (Pascussi et al., 2005), constitutive androstane receptor (Moreau et al., 2007), and silencing mediator for retinoid and thyroid hormone receptors (Konno et al., 2009). A recent study also reported that the DNA methylation status affects the basal and VDR-dependent promoter activity of CYP24 (Chung et al., 2007; Novakovic et al., 2009). Cui et al. (2009) recently reported

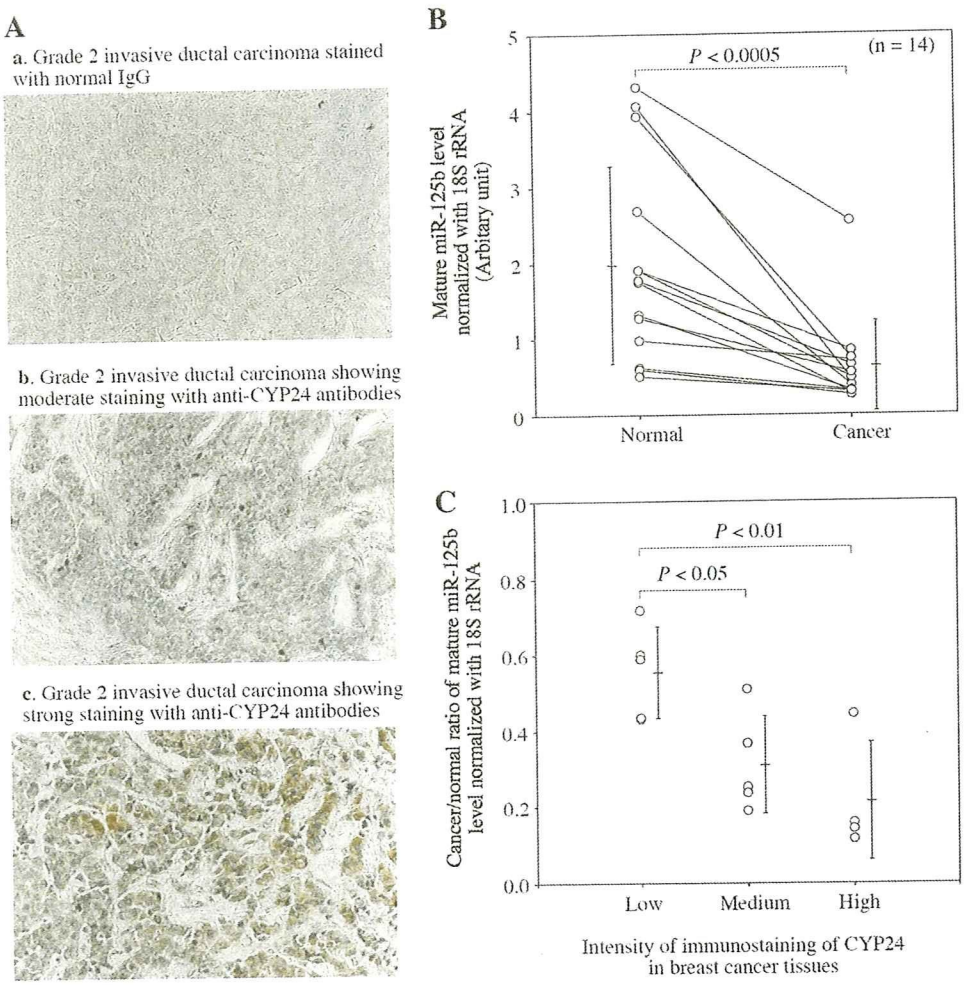

Fig. 5. Expression levels of CYP24 protein and miR-125b in human breast cancer tissues. A, immunohistochemical staining of CYP24 protein in breast cancer tissues. a, grade 2 invasive ductal carcinoma with normal IgG showed no staining. b, grade 2 invasive ductal carcinoma with anti-human CYP24 showed medium staining. c, grade 2 invasive ductal carcinoma with anti-human CYP24 showed high staining. B, the expression levels of mature miR-125b in breast cancer tissues and adjacent normal tissues obtained from 14 patients were determined by real-time RT-PCR. The expression levels were normalized with the 18S rRNA level. Horizontal and vertical bars represent the mean ± S.D. C, the relationship between the CYP24 protein levels in breast cancer tissues and the cancer/normal ratio of mature miR-125b levels.

that the extracellular signal-regulated kinase signaling pathway is involved in the $1,25(OH)_2D_3$-mediated CYP24 induction. In addition to these transcriptional regulation mechanisms, we found that the CYP24 expression is post-transcriptionally regulated by miRNA. Thus, this study provides new insight into the regulation mechanisms of human CYP24.

This is the first report, to our knowledge, demonstrating by immunohistochemistry that CYP24 protein is elevated in human breast cancer tissues. The increased expression of CYP24 would be due to the decreased expression of miR-125b in human breast cancer tissues. Mature miR-125b is formed by two precursors, miR-125b-1 and miR-125b-2, which are located in chromosomes 11q24.1 and 21q11.2, respectively (http://microrna.sanger.ac.uk/sequences/). It has been reported that the chromosome regions 11q23–24 (Negrini et al., 1995) and 21q11–21 (Yamada et al., 2008) are frequently deleted in breast cancers. This could be one of the mechanisms of the down-regulation of miR-125b in breast cancer.

We have found that human VDR is also regulated by miR-125b (Mohri et al., 2009). Therefore, the up-regulation of VDR in breast cancer by the down-regulation of miR-125b may partly contribute to the up-regulation of CYP24. The increase of CYP24 level would attenuate antitumor activity of $1,25(OH)_2D_3$. In contrast, the increase of VDR level would augment the antitumor activity of $1,25(OH)_2D_3$. In our recent study (Mohri et al., 2009), we investigated the effects of miR-125b on the antiproliferative effects of $1,25(OH)_2D_3$ by evaluating the growth of MCF-7 cells. We found that the cell growth was significantly inhibited by $1,25(OH)_2D_3$; however, the inhibited cell growth was prominently diminished by the overexpression of miR-125b (Mohri et al., 2009). Accordingly, the effects of miR-125b could be stronger for VDR than for CYP24 in this breast cancer cell line. A possible explanation for this observation is that the CYP24 protein level in the MCF-7 cells might be too low to inactivate the exogenously added $1,25(OH)_2D_3$.

The miR-125b has been considered to be a tumor suppressor gene, because it can suppress the expression of *ERBB2* and *ERBB3* oncogenes (Scott et al., 2007). In addition, it has been reported that miR-125b inhibited the cell proliferation of human breast cancer cells (Scott et al., 2007), hepatocellular carcinoma cells (Li et al., 2008), and thyroid carcinoma cells (Visone et al., 2007). In contrast, Lee et al. (2005) reported that inhibition of miR-125b resulted in the decrease of growth of human prostate cancer cells. Because the miR-125b expression differently changes in human tumors and that the miR-125b is down-regulated in breast, ovarian, and bladder cancers but is up-regulated in pancreas and stomach cancers (Volinia et al., 2006), it can be hypothesized that the miR-125b acts in different ways depending on the cellular context. Mizuno et al. (2008) have recently reported that miR-125b is involved in osteoblastic differentiation through the regulation of cell proliferation. Because we found the role of miR-125b in controlling the level and action of $1,25(OH)_2D_3$, it is also interesting to know the function of miR-125b for normal calcium and bone homeostasis in the future.

In the miRNA field, rapid progress has been made in the previous half-decade. The roles of miRNA in biological processes such as cell proliferation, development, and apoptosis as well as in various diseases such as cancer, cardiovascular diseases, and Alzheimer's disease have become recognized (Erson and Petty, 2008; Garofalo et al., 2008). Information concerning the targets of miRNA is increasing. However, among a large number of cytochrome P450 isoforms, the currently known isoforms that were identified as targets of miRNA are only human CYP1B1 (Tsuchiya et al., 2006), rat CYP2A3 (Kalscheuer et al., 2008), and human CYP24 in this study. Further studies are required to understand the contribution of miRNAs to the regulation of drug-metabolizing enzymes in relation to their physiological roles.

In conclusion, we found that human CYP24 is post-transcriptionally regulated by miR-125b, which would serve as a possible mechanism for the high CYP24 expression in cancer tissues. This study could provide new insight into the regulatory mechanism of human CYP24.

Acknowledgments

We greatly appreciate the enthusiasm and research support of Noriko Kawagishi (Futaba Breast Clinic). We are grateful to Dr. Toshiyuki Sakaki, Toyama Prefectural University, for providing recombinant human CYP24 as a positive control. We acknowledge Brent Bell for reviewing the manuscript.

References

Albertson DG, Ylstra B, Segraves R, Collins C, Dairkee SH, Kowbel D, Kuo WL, Gray JW, and Pinkel D (2000) Quantitative mapping of amplicon structure by array CGH identifies CYP24 as a candidate oncogene. *Nat Genet* **25**:144–146.

Anderson MG, Nakane M, Ruan X, Kroeger PE, and Wu-Wong JR (2006) Expression of VDR and CYP24A1 mRNA in human tumors. *Cancer Chemother Pharmacol* **57**:234–240.

Bartel DP (2004) MicroRNAs: genomics, biogenesis, mechanism, and function. *Cell* **116**:281–297.

Calin GA, Sevignani C, Dumitru CD, Hyslop T, Noch E, Yedamuri S, Shimizu M, Rattan S, Bullrich F, Negrini M, et al. (2004) Human microRNA genes are frequently located at fragile sites and genomic regions involved in cancers. *Proc Natl Acad Sci USA* **101**:2999–3004.

Chen KS and DeLuca HF (1995) Cloning of the human 1α,25-dihydroxyvitamin D-3 24-hydroxylase gene promoter and identification of two vitamin D-responsive elements. *Biochim Biophys Acta* **1263**:1–9.

Chung I, Karpf AR, Muindi JR, Conroy JM, Nowak NJ, Johnson CS, and Trump DL (2007) Epigenetic silencing of CYP24 in tumor-derived endothelial cells contributes to selective growth inhibition by calcitriol. *J Biol Chem* **282**:8704–8714.

Cui M, Zhao Y, Hance KW, Shao A, Wood RJ, and Fleet JC (2009) Effects of MAPK signaling on 1,25-dihydroxyvitamin D-mediated CYP24 gene expression in the enterocyte-like cell line, Caco-2. *J Cell Physiol* **219**:132–142.

Deeb KK, Trump DL, and Johnson CS (2007) Vitamin D signalling pathways in cancer: potential for anticancer therapeutics. *Nat Rev Cancer* **7**:684–700.

de Lyra EC, da Silva IA, Katayama ML, Brentani MM, Nonogaki S, Góes JC, and Folgueira MA (2006) $25(OH)D_3$ and $1,25(OH)_2D_3$ serum concentration and breast tissue expression of 1α-hydroxylase, 24-hydroxylase and Vitamin D receptor in women with and without breast cancer. *J Steroid Biochem Mol Biol* **100**:184–192.

Erson AE and Petty EM (2008) MicroRNAs in development and disease. *Clin Genet* **74**:296–306.

Garofalo M, Condorelli G, and Croce CM (2008) MicroRNAs in diseases and drug response. *Curr Opin Pharmacol* **8**:661–667.

Hicks J, Krasnitz A, Lakshmi B, Navin NE, Riggs M, Leibu E, Esposito D, Alexander J, Troge J, Grubor V, et al. (2006) Novel patterns of genome rearrangement and their association with survival in breast cancer. *Genome Res* **16**:1465–1479.

Iorio MV, Ferracin M, Liu CG, Veronese A, Spizzo R, Sabbioni S, Magri E, Pedriali M, Fabbri M, Campiglio M, et al. (2005) MicroRNA gene expression deregulation in human breast cancer. *Cancer Res* **65**:7065–7070.

Kallioniemi A, Kallioniemi OP, Piper J, Tanner M, Stokke T, Chen L, Smith HS, Pinkel D, Gray JW, and Waldman FM (1994) Detection and mapping of amplified DNA sequences in breast cancer by comparative genomic hybridization. *Proc Natl Acad Sci U S A* **91**:2156–2160.

Kalscheuer S, Zhang X, Zeng Y, and Upadhyaya P (2008) Differential expression of microRNAs in early-stage neoplastic transformation in the lungs of F344 rats chronically treated with the tobacco carcinogen 4-(methylnitrosamino)-1-(3-pyridyl)-1-butanone. *Carcinogenesis* **29**:2394–2399.

Konno Y, Kodama S, Moore R, Kamiya N, and Negishi M (2009) Nuclear xenobiotic receptor pregnane X receptor locks corepressor silencing mediator for retinoid and thyroid hormone receptors (SMRT) onto the *CYP24A1* promoter to attenuate vitamin D_3 activation. *Mol Pharmacol* **75**:265–271.

Lee YS, Kim HK, Chung S, Kim KS, and Dutta A (2005) Depletion of human micro-RNA miR-125b reveals that it is critical for the proliferation of differentiated cells but not for the down-regulation of putative targets during differentiation. *J Biol Chem* **280**:16635–16641.

Lewis BP, Burge CB, and Bartel DP (2005) Conserved seed pairing, often flanked by adenosines, indicates that thousands of human genes are microRNA targets. *Cell* **120**:15–20.

Li W, Xie L, He X, Li J, Tu K, Wei L, Wu J, Guo Y, Ma X, Zhang P, et al. (2008) Diagnostic and prognostic implications of microRNAs in human hepatocellular carcinoma. *Int J Cancer* **123**:1616–1622.
Lu J, Getz G, Miska EA, Alvarez-Saavedra E, Lamb J, Peck D, Sweet-Cordero A, Ebert BL, Mak RH, Ferrando AA, et al. (2005) MicroRNA expression profiles classify human cancers. *Nature* **435**:834–838.
Medina PP and Slack FJ (2008) microRNAs and cancer: an overview. *Cell Cycle* **7**:2485–2492.
Mimori K, Tanaka Y, Yoshinaga K, Masuda T, Yamashita K, Okamoto M, Inoue H, and Mori M (2004) Clinical significance of the overexpression of the candidate oncogene CYP24 in esophageal cancer. *Ann Oncol* **15**:236–241.
Mizuno Y, Yagi K, Tokuzawa Y, Kanesaki-Yatsuka Y, Suda T, Katagiri T, Fukuda T, Maruyama M, Okuda A, Amemiya T, et al. (2008) miR-125b inhibits osteoblastic differentiation by down-regulation of cell proliferation. *Biochem Biophys Res Commun* **368**:267–272.
Mohri T, Nakajima M, Takagi S, Komagata S, and Yokoi T (2009) MicroRNA regulates human vitamin D receptor. *Int J Cancer* **125**:1328–1333.
Moreau A, Maurel P, Vilarem MJ, and Pascussi JM (2007) Constitutive androstane receptor-vitamin D receptor crosstalk: consequence on *CYP24* gene expression. *Biochem Biophys Res Commun* **360**:76–82.
Negrini M, Rasio D, Hampton GM, Sabbioni S, Rattan S, Carter SL, Rosenberg AL, Schwartz GF, Shiloh Y, and Cavenee WK (1995) Definition and refinement of chromosome 11 regions of loss of heterozygosity in breast cancer: identification of a new region at 11q23.3. *Cancer Res* **55**:3003–3007.
Nishi Y, Yanase T, Mu Y, Oba K, Ichino I, Saito M, Nomura M, Mukasa C, Okabe T, Goto K, et al. (2001) Establishment and characterization of a steroidogenic human granulose-like tumor cell line, KGN, that expresses functional follicle-stimulating hormone receptor. *Endocrinology* **142**:437–445.
Novakovic B, Sibson M, Ng HK, Manuelpillai U, Rakyan V, Down T, Beck S, Fournier T, Evain-Brion D, Dimitriadis E, et al. (2009) Placenta-specific methylation of the vitamin D 24-hydroxylase gene: implications for feedback autoregulation of active vitamin D levels at the fetomaternal interface. *J Biol Chem* **284**:14838–14848.
Pascussi JM, Robert A, Nguyen M, Walrant-Debray O, Garabedian M, Martin P, Pineau T, Saric J, Navarro F, Maurel P, et al. (2005) Possible involvement of pregnane X receptor-enhanced CYP24 expression in drug-induced osteomalacia. *J Clin Invest* **115**:177–186.
Scott GK, Goga A, Bhaumik D, Berger CE, Sullivan CS, and Benz CC (2007) Coordinate suppression of ERBB2 and ERBB3 by enforced expression of microRNA miR-125a or miR-125b. *J Biol Chem* **282**:1479–1486.
Townsend K, Banwell CM, Guy M, Colston KW, Mansi JL, Stewart PM, Campbell MJ, and Hewison M (2005) Autocrine metabolism of vitamin D in normal and malignant breast tissue. *Clin Cancer Res* **11**:3579–3586.
Tsuchiya Y, Nakajima M, Kyo S, Kanaya T, Inoue M, and Yokoi T (2004) Human CYP1B1 is regulated by estradiol via estrogen receptor. *Cancer Res* **64**:3119–3125.
Tsuchiya Y, Nakajima M, Takagi S, Taniya T, and Yokoi T (2006) MicroRNA regulates the expression of human cytochrome P450 1B1. *Cancer Res* **66**:9090–9098.
Visone R, Pallante P, Vecchione A, Cirombella R, Ferracin M, Ferraro A, Volinia S, Coluzzi S, Leone V, Borbone E, et al. (2007) Specific microRNAs are downregulated in human thyroid anaplastic carcinomas. *Oncogene* **26**:7590–7595.
Volinia S, Calin GA, Liu CG, Ambs S, Cimmino A, Petrocca F, Visone R, Iorio M, Roldo C, Ferracin M, et al. (2006) A microRNA expression signature of human solid tumors defines cancer gene targets. *Proc Natl Acad Sci U S A* **103**:2257–2261.
Wang B, Love TM, Call ME, Doench JG, and Novina CD (2006) Recapitulation of short RNA-directed translational gene silencing in vitro. *Mol Cell* **22**:553–560.
Yamada H, Yanagisawa K, Tokumaru S, Taguchi A, Nimura Y, Osada H, Nagino M, and Takahashi T (2008) Detailed characterization of a homozygously deleted region corresponding to a candidate tumor suppressor locus at 21q11–21 in human lung cancer. *Genes Chromosomes Cancer* **47**:810–818.

Address correspondence to: Dr. Tsuyoshi Yokoi, Drug Metabolism and Toxicology, Faculty of Pharmaceutical Sciences, Kanazawa University, Kakuma-machi, Kanazawa 920-1192, Japan. E-mail: tyokoi@kenroku.kanazawa-u.ac.jp

Toxicology in Vitro 23 (2009) 1179–1187

Contents lists available at ScienceDirect

Toxicology in Vitro

journal homepage: www.elsevier.com/locate/toxinvit

Establishment of knockdown of superoxide dismutase 2 and expression of CYP3A4 cell system to evaluate drug-induced cytotoxicity

Yukitaka Yoshikawa, Hiroko Hosomi, Tatsuki Fukami, Miki Nakajima, Tsuyoshi Yokoi *

Drug Metabolism and Toxicology, Faculty of Pharmaceutical Sciences, Kanazawa University, Kakuma-machi, Kanazawa 920-1192, Japan

ARTICLE INFO

Article history:
Received 14 March 2009
Accepted 28 May 2009
Available online 6 June 2009

Keywords:
Superoxide dismutase 2
CYP3A4
Cytotoxicity
RNA interference
Reactive oxygen species

ABSTRACT

Drug-induced hepatotoxicity is a major problem in drug development, and oxidative stress is known as one of the causes. Superoxide dismutases (SODs) are important antioxidant enzymes against reactive oxygen species (ROS). Mitochondria are the major source of superoxide production, and SOD2 is mainly localized in mitochondria and, with other SODs, plays an important role in scavenging superoxide. In this study, we established SOD2-knockdown cells. An adenovirus vector with short hairpin RNA against rat SOD2 (AdSOD2-shRNA) was constructed, and infection of AdSOD2-shRNA to rat hepatic BRL3A cells resulted in significant decreases of SOD2 mRNA and protein by 60%, and SOD2 activity by 50% after 3 days infection. We previously constructed an adenovirus expressing cytochrome P450 3A4 (AdCYP3A4). Co-infection of AdSOD2-shRNA and AdCYP3A4 to BRL3A cells was carried out to evaluate the superoxide- and CYP3A4-mediated formation of active metabolites, and mitochondrial toxicity, ROS and superoxide radical production and lipid peroxidation were selected to assess the cell viability. Albendazole, carbamazepine, dapsone, flutamide, isoniazid, nifedipine, sulfamethoxazole, trazodone, troglitazone, and zidovudine demonstrated significant increases of SOD2- and CYP3A4-mediated cytotoxicity. In conclusion, we constructed a highly sensitive cell system to evaluate oxidative stress and CYP3A4 mediated cytotoxicity that could be useful in preclinical drug development.

1. Introduction

Oxidative stress is one of the causes of drug-induced hepatotoxicity (Kaplowitz, 2005) and is induced by superoxide. Superoxide is mainly generated in mitochondria. Superoxide can react with NO to form peroxynitrite or, after conversion to hydrogenperoxide, undergo metal-catalysed Fenton reactions to form highly reactive hydroxyl radicals (Boelsterli et al., 2006). Superoxide dismutases (SODs) are the first and most important line of antioxidant enzyme defense systems against reactive oxygen species (ROS) and particularly superoxide anion radicals (Zelko et al., 2002). At present, three distinct SOD isoforms, SOD1, SOD2, and SOD3, have been identified in mammals. SOD1, SOD2 and SOD3 are mainly localized to the cytoplasm, mitochondria and plasma, respectively (Zelko et al., 2002). In addition, SOD2 is known to be induced by a wide variety of compounds, including lipopolysaccharide and anticancer drugs (Visner et al., 1990; Das et al., 1998). Meanwhile, the importance of SOD2 function in mammalian organisms was confirmed by disruption of the SOD2 gene, which turns out to be lethal for mice due to neurodegeneration and damage to the heart (Lebovitz et al., 1996). These suggest that SOD2 plays an especially important role in detoxification.

Recently, recombinant adenovirus methods are being developed and used for the purpose of gene delivery (Akai et al., 2007; Pérez and Cederbaum, 2003; Hosomi et al., submitted). Furthermore, a small interfering RNA strategy, which has been proven to be more specific and efficient than the full-length antisense cDNA strategy, has been established (Meister and Tuschl, 2004). In the present study, we constructed a recombinant adenovirus expressing SOD2-short hairpin RNA (AdSOD2-shRNA) that could knockdown rat SOD2 mRNA efficiently. In general, since cytochrome P450 (CYPs) are hardly expressed in cell lines, we infected adenovirus expressing CYP3A4 (AdCYP3A4). CYP3A4 is the dominant CYP3A enzyme in the liver and intestine (Rendic and Di Carlo, 1997; Shimada et al., 1994), and contributes to the metabolism of more than 50% of drugs clinically in use today (Rendic and Di Carlo, 1997; Nelson, 1999; Guengerich, 2001). In addition, metabolic activations of drugs by CYP3A4 are thought to induce hepatotoxicity (Vignati et al., 2005). Based on these considerations, in the present study we established an SOD2-knockdown and CYP3A4-expressing cell system to evaluate the oxidative stress and the CYP3A4-mediated cytotoxicity with high sensitivity for preclinical drug development studies.

* Corresponding author. Tel./fax: +81 76 234 4407.
E-mail address: tyokoi@kenroku.kanazawa-u.ac.jp (T. Yokoi).

0887-2333/$ - see front matter © 2009 Elsevier Ltd. All rights reserved.
doi:10.1016/j.tiv.2009.05.024

2. Materials and methods

2.1. Materials

Cell Counting Kit-8s (CCK-8) for 3-(4,5-dimethylthiazol-2-yl)-2,5-diphenyl tetrazolium bromide (MTT) assay, testosterone, corticosterone, carbamazepine, dantrolene, flutamide, nifedipine, sulfamethoxazole, trazodone, and zidovudine were obtained from Wako Pure Chemical Industries (Osaka, Japan). Troglitazone and rosiglitazone were kindly provided by Daiichi-Sankyo (Tokyo, Japan). Albendazole, dapsone, isoniazid, nimesulide, and 2,7-dihydro dichlorofluorescein (DCF) were obtained from Sigma–Aldrich (St. Louis, MO). ReverTra Ace (Moloney Murine Leukemia Virus Reverse Transcriptase RNaseH Minus) was from Toyobo (Tokyo, Japan). The Adenovirus Expression Vector kit (Dual Version), RNAiso, random hexamer and SYBR Premix Ex Taq were obtained from Takara (Osaka, Japan). The QuickTiter Adenovirus Titer Immunoassay kit was obtained from Cell Biolabs (Tokyo, Japan). Lipofectamine 2000 and α-minimum essential medium were obtained from Invitrogen (Grand Island, NY). The GeneSilencer shRNA Vector kit was obtained from Gene Therapy Systems (San Diego, CA). Dulbecco's modified Eagle's medium and Ham's F12 medium were obtained from Nissui Pharmaceutical (Tokyo, Japan). All primers and oligonucleotides for shRNA were commercially synthesized at Hokkaido System Sciences (Sapporo, Japan). Lipid peroxidation measurement kit was obtained from BIOMOL (Philadelphia, USA). Other chemicals were of analytical or the highest grade commercially available.

2.2. Design of short hairpin RNA

Rat SOD2 (Gene Bank™, accession code NM_017051 Gene bank) knockdown was achieved by RNA interference using an adenovirus vector-based short hairpin RNA (shRNA) approach. The sequences of shRNA-targeted SOD2 cDNA were designed by B-Bridge (Mountain View, CA). The sequences of SOD2-shRNA are: top strand, 5′-gatccCCACATATGTGTAAGCATAgaagcttgTATGCTTACACATATGTGG-3′, and bottom strand, 5′-ggccgcttccaaaaaaCCACATATGTGTAAGCATAcaagcttcTATGCTTACACATATGTGGg-3′. As a negative control, the oligonucleotide sequences of the shRNA target for luciferase from a GeneSilencer shRNA Vector kit were used.

2.3. Recombinant adenovirus

To generate the recombinant adenovirus vector expressing SOD2-shRNA (AdSOD2-shRNA), pGSU6-GFP plasmids were recombined into the pAxcwit using the cosmid-terminal protein complex (COS-TPC) method according to the manufacturer's instructions. In brief, double strand oligo DNA for shRNA of SOD2 was inserted into the *Bam*HI and *Not*I sites of the pGSU6-GFP vector. This product was digested by *Hinc*II and inserted into the *Swa*I site of the pAxcwit vector. In a similar way, the recombinant adenovirus vector expressing CYP3A4 was generated (Hosomi et al., submitted). CYP3A4 cDNA was inserted into the *Swa* I sites of the pAxCAwtit using the COS-TPC method. This pAxcwit or pAxCAwtit vector and the parental adenovirus DNA terminal protein complex were co-transfected into 293 cells by lipofectamine 2000. The recombinant adenovirus was isolated and propagated into the 293 cells. Then, adenoviruses containing shRNA of SOD2 or CYP3A4 were constructed. As a negative control, the oligonucleotide sequences of the shRNA target for luciferase from a GeneSilencer shRNA Vector kit were used (AdLuc-shRNA). The titer was determined by a QuickTiter Adenovirus Titer Immunoassay kit. The titers of Ad-SOD2-shRNA, AdCYP3A4, and AdLuc-shRNA were 1.0×10^9 pfu/mL, 7.4×10^9 pfu/mL, and 1.0×10^{10} pfu/mL, respectively.

2.4. Cell culture

The 293 cell line, rat hepatic cell line BRL3A, and rat hepatoma cell line H4IIE were obtained from American Type Culture Collection (Manassas, VA). The human hepatoma cell line HLE was obtained from the Japanese Collection of Research Biosources (Tokyo, Japan). The mouse hepatoma cell line Hepa1–6 was kindly provided by Dr. S. Kaneko (Kanazawa University, Japan). The 293 cell line was maintained in Dulbecco's modified Eagle's medium containing 10% fetal bovine serum (BioWhitaker, Walkersville, MD), 3% glutamine, 16% sodium bicarbonate, and 0.1 mM nonessential amino acids (Invitrogen) in a 5% CO_2 atmosphere at 37 °C. BRL3A cells were maintained in Ham's F12, HLE and Hepa1–6 cells were maintained in Dulbecco's modified Eagle's medium, and H4IIE cells were maintained in α-minimal essential medium. All cell lines were infected by the adenovirus in medium containing 5% fetal bovine serum.

2.5. Real time reverse transcription (RT)-PCR analysis

RNA from the hepatic cells was isolated using RNAiso. Rat SOD2 and glyceraldehyde-3-phosphate dehydrogenase (GAPDH) were quantified by real-time RT-PCR. Primer sequences used in this study were as follows: rat SOD2, 5′-GAGGCTATCAAGCGTGACTTTGG-3′ and 5′-AAGCGTGCTCCCACACATCAATC-3′; mouse SOD2, 5′-AGATCATGCAGCTGCACCACA G-3′ and 5′-GCTTGATAGCCTCCAGCAACTC-3′; human SOD2, 5′-CAGATAGCTCTTCAGCCTGCAC-3′ and 5′-GAGCCTTGGACACCAACAGAT-3′; rat GAPDH, 5′-GTTACCAGGGCTGCCTTCTC-3′ and 5′-GGGTTTCCCGTTGATGACC-3′; mouse GAPDH, 5′-TCACCAGGGCTGCCATTTG-3′ and 5′-CTCACCCCATTTGATGTTAGT-3′; human GAPDH, 5′-CCAGGGCTGCTTTTAACTC-3′ and 5′-GCTCCCCCCTGCAAATGA-3′. For the reverse transcription process, total RNA (2 μg) and 150 ng of random hexamer were mixed and incubated at 70 °C for 10 min. RNA solution was added to a reaction mixture containing 100 units of ReverTra Ace, reaction buffer, and 0.5 mM dNTPs in a final volume of 40 μl. The reaction mixture was incubated at 30 °C for 10 min, 42 °C for 1 h, and heated at 98 °C for 10 min to inactivate the enzyme. The real-time RT-PCR was performed using a Smart Cycler (Cepheid, Sunnyvale, CA). The PCR mixture contained 1 μl of template cDNA, SYBR Premix Ex Taq solution, and 10 pmol of sense and antisense primers. The PCR conditions for GAPDH and SOD2 were as follows, after an initial denaturation at 95 °C for 30 s, the amplification was performed by denaturation at 94 °C for 4 s, annealing and extension at 64 °C for 20 s for 45 cycles. Amplified products were monitored directly by measuring the increase of the dye intensity of the SYBR Green I (Molecular Probes, Eugene, OR) that binds to double strand DNA amplified by PCR.

2.6. Western blot analysis

The BRL3A cell lysates (10 μg) were separated on 15% SDS-polyacrylamide gels and transferred onto polyvinylidene difluoride membrane (Immobilon-P; Millipore). The specific proteins were detected by rabbit anti-human SOD2 polyclonal antibody, cross-reacting to rat SOD2 (sc-30080; Santa Cruz Biotechnology, Santa Cruz, CA) at a dilution of 1:200. The protein bands were developed by biotinylated second antibody–peroxidase reaction. The quantitative analysis of protein expression was performed using ImageQuant TL Image Analysis software (Amersham Biosciences).

2.7. SOD2 Activity

The enzyme activity of SOD2 was measured in 1 μg of protein in the mitochondria fraction of BRL3A cells using a kit from Cayman Chemical (Funakoshi, Tokyo, Japan). The method utilizes tetrazolium salt to quantify superoxide radicals generated by xanthine

oxidase and hypoxanthine. The standard curve was generated using a quality controlled SOD standard. SOD2 activity was determined by performing the assay in the presence of potassium cyanide to inhibit SOD1, and thus measuring the residual SOD2 activity.

2.8. CYP3A4 Activity

BRL3A cells (3×10^5 cells/well) were seeded in 12 well plates. After 24 h, cells were infected with AdCYP3A4 and AdSOD2-shRNA or AdCYP3A4 alone. After 3 days, cells were incubated with 100 μM testosterone for 1 h. The concentration of 6β-hydroxytestosterone in the medium was measured using a high performance liquid chromatography (HPLC) method. Corticosterone (20 μM) was added as an internal standard. After extraction and centrifugation, the resulting supernatant was evaporated under nitrogen. The residue was diluted with 45% methanol as necessary before being injected into HPLC. Testosterone and its metabolite, 6β-hydroxytestosterone, were separated in Mightysil RP-18 column (4.6 × 150 mm; 5 μm, Kanto Chemical, Tokyo, Japan). Testosterone and 6β-hydroxytestosterone, eluted with 50% methanol/10 mM Kpi (pH 7.4) at a flow rate of 1.0 ml/min, were monitored at 240 nm.

2.9. MTT assay

To evaluate the cytotoxicity, MTT assay was performed as follows. BRL3A cells (8×10^3 cells/well) were seeded in 96 well plates. After 24 h, cells were infected with AdLuc-shRNA, AdSOD2-shRNA, and AdCYP3A4. Two days after infection, the cells were treated with albendazole, carbamazepine, dantrolene, dapsone, flutamide, isoniazid, nifedipine, nimesulide, sulfamethoxazole, trazodone, troglitazone, rosiglitazone, or zidovudine for 24 h, respectively. After 24 h, MTT was added, and absorbance at 405 nm was measured. Percent cell viability was calculated by comparing them to the absorbance of control.

2.10. Oxidative stress measurement

ROS production was estimated by the measurement of DCF fluorescence. BRL3A the cells (8×10^3 cells/well) were seeded in 96 well plates. After 24 h incubation, cells were infected with AdLuc-shRNA, AdSOD2-shRNA, and AdCYP3A4. Two days after infection, the cells were treated with albendazole, carbamazepine, dantrolene, dapsone, flutamide, isoniazid, nifedipine, nimesulide, sulfamethoxazole, trazodone, troglitazone, rosiglitazone, or zidovudine, respectively. After 24 h, the medium was removed, and the cells were rinsed twice with PBS. The cells were then incubated with a 30 μM DCF for 2 h while shielding them from light. The cells were again washed twice with PBS and then incubated in 200 μl of PBS for 1 h. The DCF fluorescence resulting from interaction of the dye with ROS was measured at 485 nm of excitation and 538 nm of emission. Superoxide anion production was estimated by the measurement of hydroethidine (HE) fluorescence following the method of Carter et al. (1994). HE was added at a final concentration of 10 μM, and plates were incubated for 30 min. The cells were then washed, trypsinized, and resuspended in PBS and fluorescence was measured at 352 nm of excitation and 590 nm of emission.

Lipid peroxidation was measured as follows. BRL3A cells (6×10^6 cells/dish) were seeded in 10 cm^2 dish. After 24 h, cells were infected with AdLuc-shRNA, AdSOD2-shRNA, and AdCYP3A4. Two days after infection, the cells were treated with albendazole, carbamazepine, dantrolene, dapsone, flutamide, isoniazid, nifedipine, nimesulide, sulfamethoxazole, trazodone, troglitazone, rosiglitazone, or zidovudine for 24 h, respectively. After 24 h, cells of three dishes in the same group were collected. Then, lipid peroxidation was measured by using commercially available kit.

2.11. Statistical analysis

Statistical analyses were performed with a GraphPad Instat version 2.0 computer program (GraphPad Software, San Diego, CA) by student'*t*-test and Analysis of Variance (ANOVA). A value of $P < 0.05$ was considered statistically significant.

3. Results

3.1. MOI-dependent knockdown effect of AdSOD2-shRNA in BRL3A cells

To investigate the most efficient multiplicity of infection (MOI), BRL3A cells were infected with AdSOD2-shRNA at MOI 0, 5, 10, 20, 50, 100 or 200 for 3 days (Fig. 1). SOD2 mRNA was decreased MOI-dependently, but some cells began floating at MOI 200. Thus, infection at MOI 100 (70% decrease of SOD2 mRNA) could be an appropriate condition of AdSOD2-shRNA infection.

3.2. Changes of SOD2 mRNA expression in various hepatic cell lines

To investigate the knockdown effect on the cells, various hepatic cell lines were infected with AdSOD2-shRNA or AdLuc-shRNA (negative control) at MOI 100 for 3 days. Real time RT-PCR analysis was performed to measure the SOD2 mRNA expression (Fig. 2). The expression level of SOD2 mRNA was significantly decreased by about 60% in BRL3A cells, but not in H4IIE, Hepa1–6, and HLE cells, and thus BRL3A cells were used in the following experiments.

3.3. Time-dependent knockdown effect of AdSOD2-shRNA in BRL3A cells

BRL3A cells were infected with AdSOD2-shRNA at MOI 100 for 1, 2, 3 or 5 days to investigate the most efficient condition for infection. SOD2 mRNA started to decrease after 2 days of infection, and a 60% decrease was achieved after 3 days infection (Fig. 3A). The decrease of SOD2 mRNA was accompanied by a decrease in SOD2 protein after 3 days infection (Fig. 3B). The SOD2 activity was also significantly decreased by 50% after 3 days of AdSOD2-shRNA infection (Fig. 3C). After 5 days AdSOD2-shRNA infection, SOD2 mRNA, protein expression, and activity had recovered a little. These results suggested that 3 days infection would be an appropriate condition of AdSOD2-shRNA infection.

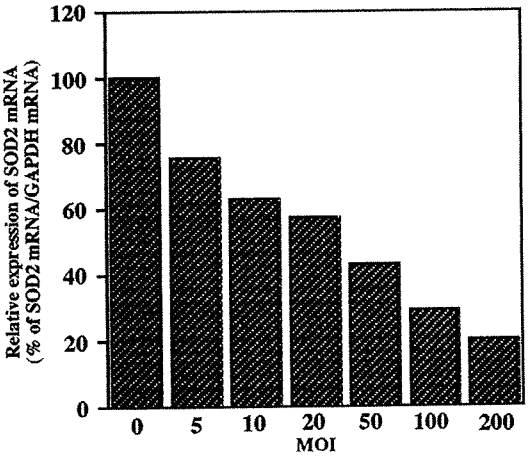

Fig. 1. MOI-dependent knockdown effect of AdSOD2-shRNA in BRL3A cells. SOD2 mRNA was determined in BRL3A cells three days after AdSOD2-shRNA infection. Data are mean of two independent experiments. The variances of the duplicate determinations were <10%.

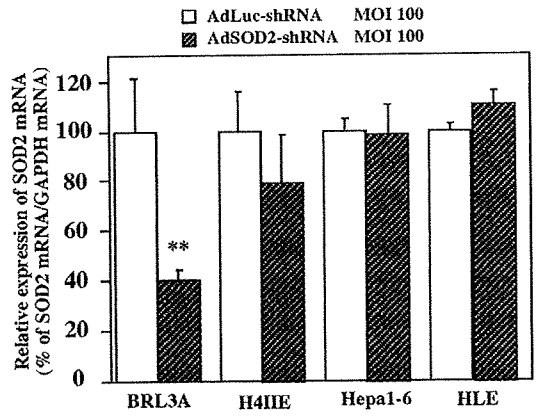

Fig. 2. Changes of SOD2 mRNA expression in various hepatic cell lines. SOD2 mRNA was determined in each cell line three days after AdSOD2-shRNA infection. Data are mean ± SD ($n = 3$). $^{**}P < 0.01$ compared with AdLuc-shRNA infected groups in each cell line. Statistical analyses were performed by student's*t*-test.

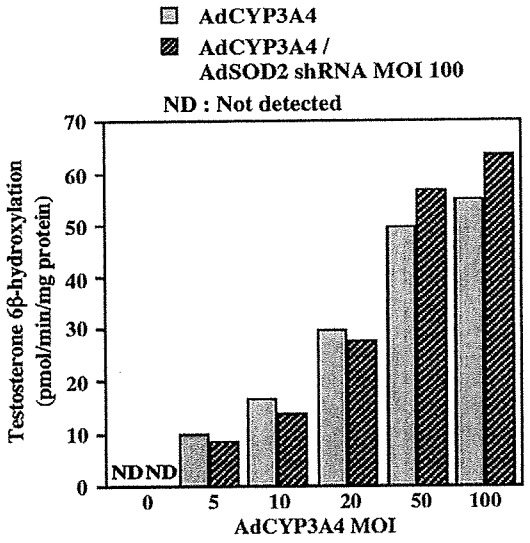

Fig. 4. AdCYP3A4 MOI-dependent expression of CYP3A4 activity in BRL3A cells. Testosterone 6β-hydroxylation was determined in BRL3A cells infected with AdCYP3A4 and/or AdSOD2-shRNA. Data are mean of two independent experiments. The variances of the duplicate determinations were <10%. ND, Not detected.

3.4. MOI-dependent expression of CYP3A4 activity in BRL3A cells

To elucidate the most appropriate condition of co-infection of AdCYP3A4 and AdSOD2-shRNA, BRL3A cells were infected with both AdCYP3A4 at MOI 0, 5, 10, 20, 50 or 100 and AdSOD2-shRNA at MOI 100 (Fig. 4). CYP3A4 activity measured by the 6β-hydroxytestosterone production was increased MOI dependently, and at MOI 50, the CYP3A4 activity nearly reached a plateau. This result suggested that the condition of co-infection of AdCYP3A4 at MOI 50 and AdSOD2-shRNA at MOI 100 would be appropriate for the cytotoxicity experiments.

3.5. MTT assay in adenovirus infected BRL3A Cells

To investigate the oxidative stress- and CYP3A4-mediated cytotoxicity of clinically used 13 drugs, BRL3A cells were infected with adenovirus. As a negative control, AdLuc-shRNA was infected at MOI 150. After 2 days infection, treatment with albendazole, carbamazepine, dantrolene, dapsone, flutamide, isoniazid, nifedipine, nimesulide, sulfamethoxazole, trazodone, troglitazone, rosiglitazone, or zidovudine was applied for 24 h (Fig. 5). By treatment with each of these drugs except dantrolene, nifedipine, nimesulide and rosiglitazone, the cell viabilities of the groups infected with both AdCYP3A4 and AdSOD2-shRNA were significantly lower than those of the groups infected with both AdCYP3A4 and AdLuc-shRNA. With nifedipine, the cell viability of the groups infected with AdSOD2-shRNA alone was significantly lower than that infected with AdLuc-shRNA. With dapsone, nifedipine, and troglitazone, the cytotoxicity in groups infected with AdCYP3A4 was enhanced compared with the groups without AdCYP3A4. With dantrolene, nimesulide and rosiglitazone, the cell viabilities of each group were not significantly changed.

3.6. Changes of ROS and superoxide productions in adenovirus infected BRL3A cells

BRL3A cells were infected with adenovirus for 2 days and then treated with the drugs used in the MTT assay for 5 or 24 h. The detection of ROS and superoxide productions was conducted at the drug concentrations demonstrating the biggest differences in cell viabilities between co-infection of AdCYP3A4 and AdSOD2-shRNA and No Ad-treatment groups (Fig. 6). By treatment with albendazole (30 μM), dapsone (30 μM), nifedipine (30 μM), sulfamethoxazole (75 μM), trazodone (75 μM), or troglitazone (50 μM) for 24 h, ROS and superoxide productions in the groups infected

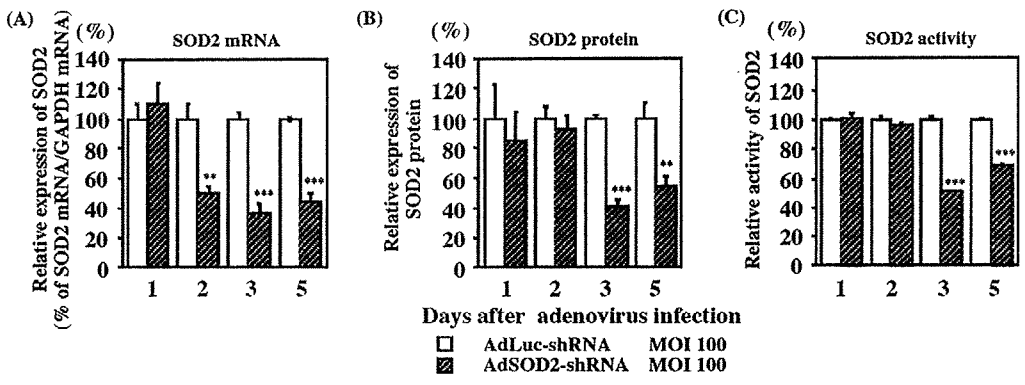

Fig. 3. Time-dependent knockdown effect of AdSOD2-shRNA in BRL3A cells. SOD2 mRNA (A) protein (B) and enzyme activity (C) were determined in BRL3A cells infected with AdLuc-shRNA or AdSOD2-shRNA. SOD2 protein was quantified by immunoblotting as described in Section 2. Data are mean ± SD ($n = 3$). $^{**}P < 0.01$, $^{***}P < 0.001$ compared with AdLuc-shRNA infected cells. Statistical analyses were performed by student's*t*-test.